The Pennsylvania State University

The Graduate School

EFFECTS OF NEURAL DEDIFFERENTIATION ON THE SELECTIVITY OF THE MAGNOCELLULAR AND PARVOCELLULAR VISUAL PATHWAYS

A Dissertation in

Psychology

by

Daniel B. Elbich

Submitted in Partial Fulfillment

of the Requirements

for the Degree of

Doctor of Philosophy

August 2020

The dissertation of Daniel B. Elbich was reviewed and approved by the following:

Nancy Dennis
Dissertation Co-Advisor
Committee Co-Chair
Associate Professor of Psychology

Reginald Adams, Jr.
Dissertation Co-Advisor
Committee Co-Chair
Professor of Psychology

Bradley Wyble
Associate Professor of Psychology

Chaleece Sandberg
Associate Professor of Communication Sciences and Disorders

Kristin Buss
Professor of Psychology and Human Development and Family Studies
Head of the Department of Psychology

ABSTRACT

One of the most marvelous aspects of the brain is that areas can be specialized to a specific duty or function. Importantly, functional specialization is widespread in the brain and can be observed in multiple different areas of cognition, especially in domain visual processing, However, across the lifespan research has identified a process known as neural dedifferentiation, whereby this specialization in brain regions declines and become less specialized for their function. In this project, I employed state-of-the-art multivariate neuroimaging methodologies to address the following questions: 1) Are there detectable differences in the neural patterns of Magnocellular and Parvocellular biased stimuli, 2) Do these patterns exhibit age-related dedifferentiation their neural response, 2A) Do patterns of dedifferentiation shift in posterior brain regions, 2B) Is there age-related dedifferentiation in the neural responses to Unbiased stimuli, 2C) Is there age-related dedifferentiation in the neural responses to facial expression, and 3) Does this dedifferentiation impact ability to detect threat in either or both visual pathways? I used a previously collected dataset of 102 adult participants spanning 60 years of healthy aging originally collected to measure threat detection. I performed multivariate pattern analyses (MVPA) to determine whether neural representations for visually biased stimuli differed along two primary visual routes, the magnocellular and parvocellular visual pathways. Secondly, these representations were interrogated to determine robustness across healthy aging. Finally, neural patterns for visually stimuli were tested for their relation to detecting facial threat. Overall the results show that neural patterns for visually biased stimuli can be observed in both the magnocellular and parvocellular visual pathways, particularly in anterior frontal and ventral temporal areas of the brain. However, there is little evidence suggesting these representations become less distinct over time or influence threat detection, suggesting that dedifferentiation may not be as ubiquitous as previously thought. This research is the first of its kind to merge visual pathway biasing, multivariate pattern classification, dedifferentiation, and social perception.

TABLE OF CONTENTS

LIST OF FIGURES

LIST OF TABLES

ACKNOWLEDGEMENTS

I would like to thank my advisor, Dr. Nancy Dennis, for her support and guidance, throughout this project and especially my graduate training. I also express my gratitude to my co-chair, Dr. Reginald Adams, Jr., for his guidance and mentorship during the dissertation process. I would like to offer special thanks to Dr. Kestutis Kveraga for his willingness to share the data set collected at Athinoula A. Martinos Center for Biomedical Imaging, Department Radiology, Massachusetts General Hospital under his supervision. Additionally, I would like to thank the other members of my committee, Dr. Bradley Wyble and Dr. Chaleece Sandberg, for their invaluable feedback and advice. I would also like to give many thanks to my colleagues in the Cognitive Aging and Neuroimaging Lab, Jordan Chamberlain and Courtney Gerver, for their help with feedback and assistance you have given me along the way. I also extend my thanks to all of the undergraduate research assistants for your help in various analysis stages for this project. I would also like to extend my heartfelt gratitude to my cohort, Drs. Federica Bulgarelli, Saskia Boggs, Leigha MacNeill, and Christina Webb, and very close friends, Dr. Eric Kamp, Ricky Groner, and Alex Webb, for all for all of their support and encouragement during my graduate career. Finally, I would like to thank my wonderful parents for their continued support.

This research was funded in part by the National Institute of Mental Health (NIMH) Grant R01 MH101194 to R. B. A., Jr. and K. K. Pursuant to Research Terms Clarification 2CFR § 200.328 (pp. 20-21), any opinions, findings, and conclusions or recommendations expressed in this publication are those of the author and do not necessarily reflect the views of the NIMH.

Chapter 1

Introduction

One of the most astonishing aspects of the brain is that areas can be specialized for a specific process or function. Importantly, functional specialization is widespread and can be observed in multiple different areas of cognition (Mishkin et al., 1983; Kanwisher et al., 1997; Poldrack et al., 2001; Adolphs, 2008; Carlezon & Thomas, 2009; Mueller, et al., 2011). However, across the lifespan research has found that this specialization declines, such that brain areas can become less specialized for their function, a process known as neural dedifferentiation (Park et al., 2004). The process of age-related dedifferentiation has been studied using different sophisticated fMRI methodologies (Park et al., 2004; Carp et al., 2011a,b; Dennis & Cabeza, 2011; Bowman et al., 2019), especially with respect to the visual system (Haxby et al., 2001; O'Toole et al., 2005; Voss et al., 2008; Carp et al., 2011b; Park et al., 2012). However, work on dedifferentiation has not yet extended to include a set of visual pathways critical for higher level visual processing, the magnocellular and parvocellular pathways. The magnocellular pathway is sensitive to high luminance contrasts and temporal changes, but cannot detect any color information nor discriminate fine detail (Kaplan & Shapley, 1986; Merigan & Maunsell, 1993). In contrast, the parvocellular pathway has low sensitivity to contrasts changes, but is color-sensitive (Kaplan & Shapley, 1986). These comprise the majority of the "where" and "what" visual streams, respectively, leaving open questions about how this impacts downstream processing, such as the detection of social visual information (Kaplan & Shapley, 1986; Merigan & Maunsell, 1993).

Specialization of Brain Function

Different areas of the brain can be thought of as being specialized for specific functions. This specialization is extensive in the brain, such as hippocampal function in memory (Olton & Paras, 1979; Chua et al., 2007; Mueller, et al., 2011), amygdalar function in threat detection and

emotion processing (Adolphs, 2008; Kosaka et al., 2002; Habel et al., 2007; Adams et al., 2011), and nucleus accumbens function for reward (Salimpoor et al., 2003; Ambroggi et al., 2008; Carlezon & Thomas, 2009). Arguably the most well-known early fMRI findings about the specialization of function was reported by Kanwisher and colleagues (1997), who reported about a functional region within fusiform gyrus that appears to hold specialization with respect to face processing (Kanwisher et al., 1997). The region, now termed the fusiform face area (FFA), is a functional region located in the fusiform gyrus that preferentially activates to faces over other categories of visual stimuli (Kanwisher et al., 1997). This finding built on previous patient work suspecting the importance of the fusiform gyrus for face-processing (De Renzi, 1977).

Findings of the circumscribed FFA resonated strongly in the literature and sparked hundreds of studies interrogating exactly how this region supports face-processing. For example, multiple studies using participants with acquired prosopagnosia (face blindness due to some form of neurological damage) show what when the area containing the fusiform is damaged or removed, individuals exhibit marked deficits in the ability to detect changes in face identity (Mundel et al., 2003; Wada & Yamamoto, 2001). In a similar vein, there have been multiple studies linking increased activation in the FFA to superior face recognition behavior, furthering the specialization of the FFA for processing of face information (Furl et al., 2011; Huang et al., 2014; Elbich & Scherf, 2017).

In addition to regions specialized for processing stimuli, research has found that certain regions are specialized for higher-order processing. For example, Poldrack and colleagues (2001) showed that different brain areas are specialized in different forms of learning and memory processing. In this study, participants were asked to learn a pattern either with trial-by-trial feedback (non-declarative memory) or were shown the correct pattern association and tested later on their learning of this knowledge (declarative memory). They reported that when the pattern was learned via feedback, activity in the basal ganglia increases while activity in the medial temporal lobe decreases. Conversely, when participants are asked to learn patterns via

associations, activity in the medial temporal lobe increases while activity in the basal ganglia decreases. These results suggest that these different forms of memory are subserved by a specialized and distinct set of regions. It also highlighted the competition and distinctiveness across the two learning systems (Poldrack et al., 2001).

Specialization within the brain is also evident in its structural architecture. One of the most widely known examples of this is ventral and dorsal visual streams, also known as the 'what' and 'where' pathways. First described in the rhesus macaque brain, the ventral pathway is located in the temporal lobe, extending from primary visual cortex and terminating at the temporal pole (Mishkin et al., 1983). This pathway is specialized for processing 'object' vision, specifically physical properties such as form, shape, and size (Mishkin et al., 1983). In contrast, the dorsal pathway, beginning again in primary visual cortex, travels through the parietal lobe, terminating in the frontal lobe (Mishkin et al., 1983). This pathway is specialized for 'spatial' vision, such as location and movement in space (Mishkin et al., 1983). Building on this early work, these dichotomous pathways have also been mapped in the human brain, showing roughly the same anatomical location and specificity to the macaque (Ungerleider & Haxby, 1994; see section *Magnocellular & Parvocellular Visual Pathways* for further discussion).

This and other similar evidence suggest that the brain is a complex network of different regions specialized for a given function or cognitive processing. This is not to say that a specific function resides in only a single brain region, but that a single brain region can be optimized for some specific task or information (e.g., FFA preference to faces over objects). Importantly, we know from developmental work that these regions and this specialization is something that develops in formative years (Kadosh & Johnson, 2007; Peelen et al., 2009). That is to say, the FFA for example, does not exhibit this specialization in early childhood, but rather specialization develops slowly over the course of childhood and adolescents through exposure to faces (Gauthier & Nelson, 2001). Similar development of neural specialization is found across other brain regions as well (Adolphs, 2003; Ofen et al., 2007; DeMaster et al., 2013). Unfortunately,

research at the other end of the age spectrum also suggests that this specialization may not be fixed throughout advanced aging.

Neural Dedifferentiation in Healthy Aging

While this neural specificity is prevalent in multiple aspects of cognition, it unfortunately is not a static quality of the brain. As humans age, there is a measurable decrease in the selectivity of brain regions with respect to the specific class of stimuli or cognitive operation they for which they are specialized (Park et al., 2004; Dennis & Cabeza, 2011; Park et al., 2012; Carp et al., 2011a,b; Burianová et al., 2013; Martins et al., 2014). This process has been coined as neural dedifferentiation (Park et al., 2004). The process of age-related dedifferentiation was originally studied in the domain of visual processing. For example, Park & colleagues (2004) showed participants images of faces, houses, chairs, pseudowords and phase scrambled images and asked to remember each image (no memory test was given afterwards) and recorded activations levels across regions in visual cortex, focusing on those regions known to support processing of each stimulus type. Mean *t* responses were taken from a subset of the most active voxels within masks of the parahippocampal gyrus, inferior temporal gyrus, and fusiform gyrus for house, word, chair, and face stimuli compared to scrambled images, respectively. This served as a value of specificity for each category. Their results showed an interaction with age wherein younger adults exhibited greater category-specificity compared to older adults. In addition, older adults had an increased number of shared voxels across each category (e.g., a voxel that was both a peak for face activation and also chair activation) compared to younger adults.

This study represents some of the first neuroimaging work to suggest that neural specificity declines with age. Since then, numerous studies have replicated age-related neural dedifferentiation in occipital cortices (e.g., Park et al., 2012; Burianová et al., 2013; Bowman et al., 2019) and even extended it to other specialized regions. For example, Dennis & Cabeza (2011) investigated age-related dedifferentiation in the domain of learning. Specifically, researchers here examined the effects of dedifferentiation on explicit and implicit memory in

different regions of the medial temporal lobe (MTL). The explicit learning task was one of encoding and subsequent recognition memory for words, whereas the implicit learning task examined implicit sequence learning. Similar to what was shown by Poldrack and colleagues (2001), the results showed that young adults preferentially recruited the MTL bilaterally during explicit learning, but were preferentially recruiting the putamen and caudate for implicit learning. Conversely, older adults showed no preferential recruitment of either areas, with mean activation being comparable across both conditions (Dennis & Cabeza, 2011). The authors took this as evidence for age-related dedifferentiation of the two learning systems. Interestingly reduced specialization was accompanied by performance benefits in older adults, such that those older adults that were able to tap into both learning systems showed higher rates of performance across the 2 learning tasks.

Finally, Carp and colleagues (2011a) examined dedifferentiation in the motor control system. Here, participants were simply asked to tap their left or right index finger, or alternate between each finger. Participants tapped in time with a metronome at a rate of 1Hz (Carp et al., 2011a). Researchers here performed multivoxel pattern analyses (MVPA; see *Understanding Specialization in the Brain* for further discussion) to quantify the pattern of activation within younger and older adults. Their results show that distinctiveness of activation to the motor task was reduced in older adults, driven by decreased within- and between-condition similarity in multiple motor regions such as bilateral primary motor cortex (M1), supplemental motor area (SMA) and the cerebellum (Carp et al., 2011a). Importantly, when controlling for gray matter volume, older adults still showed decreased distinctiveness in left M1, SMA, and the cerebellum (Carp et al., 2011a).

Taken together, these studies suggest there that age-related dedifferentiation in the brain is a broad process not limited to a specific area or region. Moreover, research suggests that dedifferentiation can be measured at the level of activation and neural representation. Yet, work

in this domain is has only just begun to understand the nuances of how exactly specialized regions become less-specific and the ramifications of this process.

Understanding Specialization in the Brain

Functional specialization of the brain was initially studied through case studies & patient populations. For example, much of the early work on how the brain processed faces came from work with acquired prosopagnosia, or face blindness (Lhermitte et al., 1972; Meadows, 1974; Damasio et al., 1982). In line with this, the contribution of subject H.M., who bilateral lesioning of the hippocampus, amygdala, and parahippocampal gyrus, led to the understanding of how structures within the medial temporal lobe are implicated in memory formation and recollection was critical (Scoville & Milner, 1957; Squire & Wixted, 2011). However, since the advent of *in-vivo* imaging techniques, functional brain specialization can now be studied in the population at large.

The most common approach to studying specialization is the use of functional magnetic resonance imaging (fMRI). This imaging technique provides incredible spatial resolution and is more commonly available in non-clinical settings compared to other imaging techniques (e.g., PET). Using fMRI, initial work focused primarily on univariate differences in brain activation, as measured by gross differences in blood flow between different regions or different functional states, in order to determine neural selectivity. The seminal paper from Kanwisher and colleagues (1997) has participants viewing images of faces, objects, houses, body parts, and scrambled images, then statistically testing within each voxel if the signal was greater for faces or other items (e.g., houses). This resulted in a set of voxels which were selective to faces over all other conditions in the fusiform gyrus and the larger finding that there is a specialized functional area within the gyrus. This particular methodology for "defining" specialization has been replicated many times over across different domains (Dennis & Cabeza, 2011; Furl et al., 2011; Huang et al., 2013; Elbich et al., 2017). While this technique is very useful, however, it is limited to simply testing relative differences in the quantity or height of activation across stimulus sets (e.g., faces

vs. houses) or cognitive conditions (e.g., explicit vs. implicit learning), as well as across groups (e.g., young vs. old adults). It does not provide any information about how the different types of information is represented in the voxels or how the pattern of activation within these voxels may differ across conditions or groups, nor in how a region is being deployed functionally.

More recently, multivariate techniques are being employed to understand functional specialization, the most prolific of which is multivoxel pattern analysis (MVPA; Norman et al., 2006). This approach uses pattern-classification to measure signal within individual voxels, not a contrast (Norman et al., 2006). The benefit here is that voxels with lower signal can contribute to characterizing the pattern, even if it would not typically reach statistical significance in a univariate approach (Norman et al., 2006). In general, this approach has four steps. First, the voxels to be tested must be determined in some manner, which is called feature selection. This can be done in multiple ways, such as using anatomy to select voxels of interest or using an independent dataset to select the most active voxels to use (Norman et al., 2006). Second, the data must be sorted with respect to their specific condition (e.g., activation to faces vs. houses). Finally, a classification algorithm must be fed this data to map voxel pattern information to a specific condition (Norman et al., 2006). Finally, the classifier must be given a novel set of data to determine if it can accurately determine the condition associated with the voxel activation (Norman et al., 2006).

The development of multivariate methods has greatly refined the study of specialization the brain. Because univariate methods focus the region as a whole (e.g., a mean beta for hundreds of voxels), they are unable to capture subtle variations with regard to the overall pattern of activation within the region itself. In addition, focusing on measuring signal from individual voxels helps to mitigate problems of signal dropout in medial brain regions and regions close to the sinuses, where poorer signal can prevent accurate detection (Ojemann et al. 1997; Schacter & Wagner, 1999; Deichmann et al., 2003). This provides a unique opportunity to investigate specialization areas of the brain that were previously difficult to isolate.

Multivariate approaches have greatly helped our understanding of functional specialization. For example, O'Toole and colleagues (2005) examined the pattern of distributed activation in the ventral temporal cortex implementing a linear classifier (e.g., early Multivariate Pattern Analysis), which was trained to determine if activation in a given voxel was more or less likely to be related to a given category (O'Toole et al., 2005). Participants were shown images of faces, houses, cats, common objects, and scrambled pictures while fMRI data was collected (Haxby et al., 2001; O'Toole et al., 2005). The images during scanning were also fed into a linear classifier to obtain similarity metrics among the images themselves, irrespective of the brain data (e.g., similarity of chair images to one another). The results showed that the degree to which a voxels shared activation across separate categories was related to the degree to which objects shared common features with one another (O'Toole et al., 2005). In other words, objects that shared more common features (e.g., different types of chairs) had similar representations in the brain (e.g., chairs compared to faces). This suggests that visual categories that share features/attributes also share some level of representation in the brain (O'Toole et al., 2005).

In addition, Bowman & colleagues (2019) investigated the specificity of memory representations in temporal and occipital cortices. Here, participants viewed common objects and were asked to respond if the item was larger or smaller than a shoebox (e.g., a black crow; Bowman et al., 2019). In a subsequent memory retrieval task, participants viewed all original images in addition to a set of item lures (e.g., a different black crow), thematic lures (e.g., a different bird), and novel lures (e.g., a shopping cart), during which participants had to respond if they remembered the item, if they felt they had seen it before but were unsure, or if felt it was new (Bowman et al., 2019). MVPA classification was performed distinguishing the targets to item lures and targets to thematic lures, respectively. The results showed that classification was only statistically above chance in the midline occipital for the target & item lure comparison, with classification accuracy being greater in young adults compared to old (Bowman et al., 2019). This suggests that neural representations for remembered items differ across different age groups, with

patterns in older adults being more similar to incorrect items. In addition, when coupled with the decreased d-prime scores in older adults, these patterns can also potentially represent different types of information for each group (Bowman et al., 2019).

Magnocellular & Parvocellular Visual Pathways

As stated above, the magnocellular and parvocellular pathways are two key visual pathways in primates which derive their names from their cellular origins. The magnocellular (magno) pathway, first discovered in the adult macaque, originates from large retinal ganglion cells which project to the deep layers (1 & 2) of the lateral geniculate nucleus (LGN) and subsequently to layer 4Ca of the primary visual cortex (Boycott & Wassle, 1991; Kaplan, 2004; Kveraga et al., 2007a). Receptor cells for this pathway have large receptive fields and are sensitive to high luminance contrasts temporal changes, but cannot detect any color information nor discriminate fine detail (see Figure 1; Kaplan & Shapley, 1986; Merigan & Maunsell, 1993). This pathway comprises the majority of the "where" visual stream, continuing from primary visual cortex through higher order attention regions in dorsal temporal and parietal cortex and ending in frontal cortex (Mishkin et al., 1983).

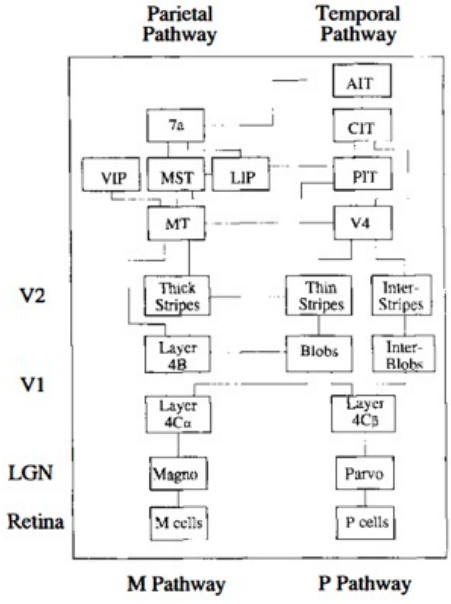

Figure 1. Diagram of the Magnocellular and Parvocellular visual pathways from Merigan & Maunsell (1993).

Similarly, the parvocellular (parvo) pathway originates from midget retinal ganglion cells which project to the shallower layers (3-6) of the lateral geniculate nucleus (LGN) and subsequently to layer 4A and 4Cb of the primary visual cortex (Callaway, 2005; Kveraga et al., 2007a). Receptor cells for this pathway have smaller receptive fields, low sensitivity to contrasts changes, but are color-sensitive (Kaplan & Shapley, 1986). This pathway comprises the majority of the "what" visual stream, continuing from primary visual cortex through higher visual regions (e.g., V2, V4), finally terminating in the inferior temporal cortex (Mishkin et al., 1983). Later stages of this pathway (outside of V1) become more sensitive to other properties of the stimulus such as viewpoint or brightness (Vogels et al.,, 2001; Qiu & von der Heydt, 2005), while other areas within the pathway become more specialized for specific classes of stimuli such as faces (Puce et al., 1995; Kanwisher et al., 1997) or objects (Ishai et al., 2000; Grill-Spector et al., 2001).

While this specialization has been studied extensively in the macaque brain, research in the human brain has not been as extensive. Because the LGN is located deep within the brain and is a relatively small structure, it is difficult to study distinct signals from magnocellular and parvocellular subdivision with noninvasive techniques more traditionally used in human subjects' research (Denison et al., 2014). However, one fMRI study was able to functionally map the magno and parvo pathways in the human brain. Denison & colleagues (2014) set out to determine if the human brain had the same functional specializations of magno and parvo pathways in the LGN as the macaque. In this study, they functionally isolated the LGN by presenting a flickering checkerboard pattern to alternating visual hemifield, akin to stimuli known to elicit a response in monkey neurons. Participants were then shown an magno-/parvo-biased localizer, with mango-biased stimuli consisting of black and white, high luminance contrast gratings and parvo stimuli being low luminance contrast, reg-green gratings (see Figure 2). Their results showed that magno-related voxels of the LGN were more ventral and medial, while parvo-related voxels were more dorsal and lateral, matching predictions from human histological studies of the LGN

(Denison et al., 2014).

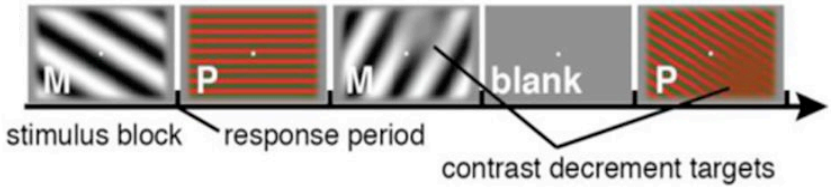

Figure 2. Example trial from Magno (magno)/Parvo (parvo) Localizer taken Denison et al., (2014).

Importantly, work in clinical populations has yielded some findings related to their functionality. For example, Murav'eva and colleagues (2009) examined lesioning at the neural level of either the magno or parvo pathway impacted visual function. Patients with multiple sclerosis (an autoimmune neurodegenerative disorder) engaged in a contrast sensitivity task where they were shown Gabor grids of different spatial frequencies gradually increasing in contrast from 0 to 1 (Murav'eva et al., 2009). Grids were presented to each eye individually seven times using a staircase procedure, where patients pressed/held a button when they could see the grid and released when they could not (Murav'eva et al., 2009). Their results show that patients exhibiting deficiencies at high contrast contrasts also showed clinical impairments to their vision (e.g., light adaptation, deterioration of daytime vision), suggesting lesion damage to the parvo pathway (Murav'eva et al., 2009). Conversely, patients showing deficiencies in the low to intermediate contrast range did not show any clinical impairments in their vision, suggesting damage to the magno pathway (Murav'eva et al., 2009). Critically, other visual and neurological disorders (e.g., Parkinson's disease, Alzheimer's disease) have linked deficiencies the magno and parvo pathways to observed symptomology, exemplifying how extensive this is in the brain (Yoonessi & Yoonessi, 2011).

Role of Magnocellular and Parvocellular Pathways in Cognition

Function of the magnocellular and parvocellular pathways can also play an important role in cognitive processes ranging from reading & phonological processing (Vidyasagar & Pammer,

1999, 2010; Ahmadi et al., 2015; Gori et al., 2016; Lawton, 2016), to motion perception (Gilmore et al., 1994), face perception (Vuilleumier & Pourtois, 2007; Awasthi et al., 2016) and threat detection (Im et al., 2017, 2018; Cushing et al., 2019; Adams et al., 2019), as well as clinical disorders such as schizophrenia (Kim et al., 2006; Martinez et al., 2008; Chieffi, 2019) and autism (McCleery et al., 2007; Sutherland & Crewther, 2010; Brown & Crewther, 2017). For example, Ahmadi and colleagues (2015) investigated these roles in participants with dyslexia who were asked to match various images in luminance. Participants also completed a judgement task where they viewed images biased toward different visual pathways and responded if an animal was present in the image (Ahmadi et al., 2015). The results showed that dyslexic participants had a greater luminance threshold than controls, meaning that control participants were better able to match images on luminance. In addition, dyslexic participants had longer reaction times when trying to identify an animal shape compared to controls, overall suggesting deficits in both magno and parvo pathways (Ahmadi et al., 2015).

Similarly, Lawton (2016) conducted a training study with dyslexic children to determine if a disruption in magnocellular function was underlying the disorder and if this could be improved. The participants engaged in different interventions to train up processing of phonological sounds, visual direction-discrimination, and word building (Lawton, 2016). Critical to this point, the visual discrimination task employed a staircase procedure during which participants were shown a grating on the display, which contained “fish-shaped” center that would move left or right for 450ms (Lawton, 2016). The participant would then respond using the left or right arrow key, beginning the next trial. The task would increase in difficulty, increasing the similarity of the window to the surrounding grating and by increasing the movements from one to two directions (Lawton, 2016). Critically, not only did performance increase on this task over time, but participants also show increases in reading rates & comprehension, attention, and visual working memory, suggesting that training improves timing sensitivity of magnocellular neurons (towards which the task is biased) which in turn improves these cognitive processes

(Lawton, 2016).

Importantly, the specialization of these pathways has been hypothesized to contribute to the perception of faces, each delivering different pieces of information (Vuilleumier & Pourtois, 2007; Awasthi et al., 2016). Vuilleumier & Pourtois (2007) have proposed that low and high spatial frequency information (LSF; HSF) are sent along different pathways, magno and parvo pathways respectively. In addition, regions in the face processing network are more sensitive to one form of information over another, such as the FFA being more sensitive to HSF information and amygdala responding to both HSF and LSF (Vuilleumier et al., 2007).

Using this distinction and the amygdala's well-researched involvement in threat/fear perceptions (Adolphs et al., 1995; Adams et al., 2003, 2011; Vuilleumier et al., 2003; Adolphs, 2008; de Gelder et al., 2014), Im and colleagues (2017) set out to study how the perceiver's anxiety influenced perceptions of clear and ambiguous threat when presented to either the magno or parvo pathway. Participants were placed in the MRI and shown either a neutral or fear face displaying clear (direct or averted gaze, respectively) or ambiguous (averted or direct gaze, respectively) biased toward either the magno pathway (gray-scaled, low luminance), parvo pathway (red-green, iso-luminance), or neither (black and white). Previous work has shown that detection of fearful expressions increases when eye gaze is averted compared to directed eye gaze (Milders et al., 2011). They were asked to respond if the image displayed was fearful or not (Figure 3). Their results showed activation in the right amygdala increased in those with higher anxiety during viewing of fearful faces displaying clear threat along magno pathway, while activation in the left amygdala increased in those with higher anxiety during viewing of fearful faces displaying ambiguous threat along parvo pathway (Im et al., 2017). This finding not only reinforces the distinction of the magno and parvo pathway in the human brain, but also illustrates its contribution to higher order cognitive tasks.

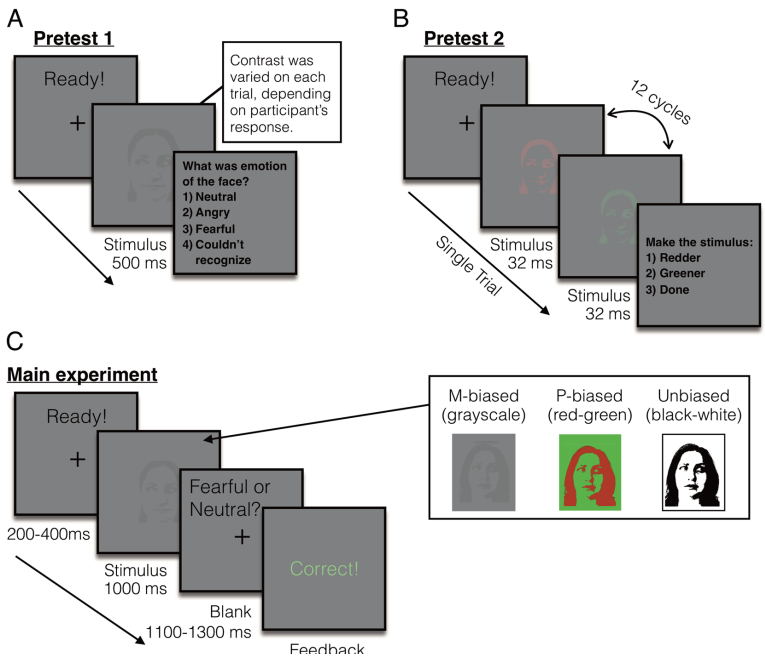

Figure 3. Example Pretest for Magno/Parvo Stimuli Creation and Experiment Trial from Im et al., 2017

Additionally, deficiencies in magnocellular pathway have been theorized as potential causes for deficits in processing visual information in some clinical disorders. For example, Kim and colleagues (2006) examined the motion perception capabilities of a sample of subjects diagnosed with schizophrenia. Motion perception/processing is located in higher order visual areas such as MT cortex, found dorsally to primary visual cortex and along the magnocellular pathway (Felleman & Van Essen, 1991; Orban et al., 2004). While measuring steady-state evoked potential using EEG, subjects engaged in a dot-motion task where perceptual thresholds for detecting coherent and incoherent motions was measured using a staircase procedure (Kim et al., 2006). These motion patterns were biased to either the magnocellular or parvocellular system (Kim et al., 2006). Once individual thresholds were determined, each subject performed an accuracy task where they were shown sequential pairs of dot-motion stimuli and simply responded “same” or “different” vocally if the pairing was the same or different (Kim et al., 2006). Their results showed that not only did those with schizophrenia have more difficulty detecting differences in the motion patterns for coherent and incoherent motion (i.e., greater

detection thresholds), amplitude during magnocellular trials decreased as the detection threshold increased (Kim et al., 2006). The parvocellular trials showed no relationship with detection threshold, suggesting input from the magnocellular pathway to the areas processing motion might be impaired (Kim et al., 2006). A similar effect was observed in a study of children with autism. In this study, children with autism performed a global/local task, which involves compartmentalizing an overall shape comprised of smaller figures (e.g., smaller boxes in the arrangement of a car), while visually evoked potentials were recorded with EEG (Brown & Crewther, 2017). Participants were asked either what picture they saw or what shape they saw in a counterbalanced order to measure global or local inspection time, respectively (Brown & Crewther, 2017). Their results showed that overall there was a trend with global inspection time (IT) and parvocellular efficiency, but interestingly in a subset of children with autism there was a sharp increase in parvocellular efficiency compared to typically developing children as measured by the peak amplitude after onset (Brown & Crewther, 2017). This finding of increased parvocellular efficiency is suggested to be the result of a compensatory mechanism for magnocellular impairment, whereby the parvocellular pathway is being engaged faster to compensate for a lagging magnocellular system (Brown & Crewther, 2017).

In sum, the magno and parvo pathways are a prime example of brain areas which are anatomically and functionally specialized. While research on these pathways in humans is still ongoing, the current state of the field suggests that the pathways can serve as important conduits for not only understanding how the human visual systems works on a fundamental level, but also how specific aspects of visual information are communicated throughout the brain.

Current Project

The specificity of neural regions is clear in human cortex and ranges across many cognitive modalities, including that of the magno and parvo pathways. It is also clear that this type of specialization declines in healthy aging. Importantly, this decline can impact higher order cognitive processes such as memory and attention. Given these two lines of evidence, it is of

interest to know whether the magnocellular and parvocellular pathways show a similar trajectory of age-related dedifferentiation and, if so, how this will impact cognitive processes that depend on the specialization. To test this, I have examined the neural specificity of the magno and parvo pathways during presentation of faces displaying threat biased towards each pathway. Using MVPA methodologies, I investigated if one or either of these pathways exhibits age-related dedifferentiation, and if this impacts the cognitive ability to accurately process threat.

1). Is there a distinction in the neural representation of Magno-/Parvo-specific stimuli along the Magnocellular and Parvocellular Pathway? I hypothesized that because neural distinction between visual stimuli is well established in the vision literature, the classifier will be able to distinguish between the representations for magno-biased and parvo-biased stimuli. This will be reflected as classification accuracy for mango-biased and parvo-biased stimuli being statistically above chance for both dorsal and ventral brain regions.

2). Is there age-related dedifferentiation in the neural responses to Magno-/Parvo-specific stimuli? I hypothesized that because age-related changes to the brain are ubiquitous and well-documented vision literature, these specialized pathways will undergo age-related dedifferentiation. This dedifferentiation would be reflected as reduced classification accuracy for parvo-specific stimuli activation in regions of the ventral visual pathway (e.g., fusiform gyrus), but not the dorsal pathway (e.g., inferior parietal), for older adults compared to younger adults. Conversely, dedifferentiation also would be reflected as reduced classification accuracy for magno-specific stimuli activation in regions of the dorsal, but not ventral, pathway for older adults compared to younger adults.

A.) Do patterns of dedifferentiation shift in posterior brain regions? I hypothesized that anterior brain regions would display greater magnitudes of dedifferentiation compared to posterior brain regions. This would be reflected as a larger reduction in classification accuracy for in frontal regions (i.e., superior frontal) for older

adults compared to younger adults, but a smaller reduction in posterior visual regions (i.e., precuneus).

B.) Is there age-related dedifferentiation in the neural responses to Unbiased stimuli? I hypothesized that because age-related changes to the brain are ubiquitous and well-documented in the vision literature and unbiased faces share visual properties with both biased conditions, these visual pathways will undergo age-related dedifferentiation for unbiased faces as well. This would be reflected as reduced classification accuracy parvo-specific/unbiased stimuli activation in regions of the ventral visual pathway (e.g., fusiform gyrus), but not the dorsal pathway (e.g., inferior parietal), for older adults compared to younger adults. Conversely, dedifferentiation also would be reflected as reduced classification accuracy for magno-specific/unbiased stimuli activation in regions of the dorsal, but not ventral, pathway for older adults compared to younger adults.

C.) Is there age-related dedifferentiation in the neural responses to facial expression? I hypothesized that because age-related changes to the brain are ubiquitous and well-documented in both vision and face processing literature, these visual pathways will exhibit age-related dedifferentiation for face expression as well. This would be reflected as reduced classification accuracy fearful/neutral parvo-biased stimuli activation in regions of the ventral visual pathway (e.g., fusiform gyrus), but not the dorsal pathway (e.g., inferior parietal), for older adults compared to younger adults. Conversely, dedifferentiation also would be reflected as reduced classification accuracy for fearful/neutral magno-specific stimuli activation in regions of the dorsal, but not ventral, pathway for older adults compared to younger adults.

3). Does this dedifferentiation impact ability to detect threat in either or both visual pathways? I hypothesized that dedifferentiation in these visual pathways will negatively impact one's ability to detect facial threat presented in their specialized modality. For example, a decreased classifier accuracy for magno-biased stimuli in dorsal regions would predict decreased

accuracy in the detection (and subsequent reporting) of threating magno-specific stimuli, but would have no relationship with parvo-specific stimuli in that same region. Similarly, decreased classifier accuracy for parvo-biased stimuli in ventral regions would predict decreased accuracy in the detection of threating parvo-specific stimuli, but would have no relationship with magno-specific stimuli in that same region.

Chapter 2

Method

General Methodology

Participants

One-hundred eight typically developing adults between ages of 19-71 years were collected[1] (see Table 1). Participants were screened for normal or corrected-to-normal vision using the Snellen eye chart to measure distance viewing, the Mars letter contrast sensitivity test to quantify ability to see visual contrast, and Ishihara color plates to test for color blindness (Snellen, 1862; Arditi, 2005; Ishihara, 1917). Written informed consent was obtained from participants using procedures approved by the Internal Review Board of the Massachusetts General Hospital, Boston, Massachusetts. Thirty-one subjects were removed in total: four for bad functional data (i.e., no signal, striations in functional maps), and 27 for poor visual cortex activation (<500 voxels). This resulted in a final sample of 77 adults ranging from 19-71 years (Table 1).

[1] It was suspected that this poor activation was a result of incorrect onset files sent to Penn State in the data transfer for a handful of subjects. Due to COVID-19 this issue could not be resolved as original data files were not accessible during quarantine. As such, data analysis was undertaken on only those subjects where onsets could be verified through data checks.

Table 1: Subject Demographics

Demographics		
	Initial	*Final*
N	108	77
Males	64	47
Females	44	30
Mean Age	38.87	38.39
Std	16.99	17.01
Range		
Min	19	19
Max	71	71

Stimuli Creation

As reported in Im et al., 2017, images for this task included 24 face identities (12 female) selected from 3 separate face databases (Ekman & Freisen, 1975; Tottenham et al., 2009; Ebner et al., 2010). Eight face identities were selected from each database to ensure even sampling. All identities had either direct or averted gaze in conjunction with either a neutral or fearful expression, resulting in 96 separate images. These images were then converted to a two-tone image (black-white) which served as both the input for the magno/parvo biasing (see below) and as face image control group (termed Unbiased).

Magnocellular Stimuli

As reported in Im et al., 2017, the appropriate luminance contrast was determined by finding the luminance threshold using a multiple staircase procedure (see Figure 3a). Participants were presented with images for 500 msec and instructed to make a key press to indicate the presented facial expression. They were required to choose one of four options: 1) neutral, 2) angry, 3) fearful, or 4) did not recognize the image. Twenty-five percent of trials were catch trials in which the stimulus did not appear. To find the threshold for foreground-background luminance contrast, the mean of the turnaround points above and below the gray background ([120 120 120] RGB value on the 8-bit scale of 0–255) were computed. From this threshold, the appropriate luminance (~3.5% Weber contrast) value was computed for the face images to be used in the low-

luminance-contrast (magno-biased) condition. As a result, the mean foreground RGB values for magno-biased stimuli were [116.5(±0.2) 116.5(±0.2) 116.5(±0.2)].

Parvocellular Stimuli

As described in Im et al., 2017, each participant's isoluminance point was determined using heterochromatic flicker photometry with two- tone face images displayed in rapidly alternating colors between red and green. The alternation frequency was ~14 Hz, as this frequency was found to obtain the best estimates for the isoluminance point (e.g., narrow range within-subjects and low variability between-subjects; Kveraga et al., 2007b; Kveraga et al., 2015; Kveraga, 2014; Thomas et al., 2012). The isoluminance point was defined as the color values at which the flicker caused by luminance differences between red and green colors disappeared and the two alternating colors fused, making the image look stable. On each trial (Figure 3b), participants were required to report whether the stimulus appeared flickering or stable using a key press. Depending on the participant's response, the value of the red gun in [r g b] was increased or decreased in a pseudorandom manner for the next cycle. The average of the values in the narrow range when a participant reported a stable stimulus became the isoluminance value for the subject used in the experiment. Thus, isoluminant stimuli were defined only by chromatic contrast between foreground and background, which appeared equally bright to the observer. The average foreground red value was 151.7(±5.35) on the background with green value of 140.

Procedure

The purpose of the study was to measure the detection of threat during the processing of magno- & parvo-biased stimuli. To do so, the study employed a fast event-related design, in which participants viewed a variable fixation of 200-400ms followed by the stimulus presentation. Following fixation, the face stimulus (magno-biased, parvo-biased, or unbiased) was presented for 1000ms followed by a variably blanks screen of 1100-1300ms (Figure 3c). Participants were asked to respond as quickly as possible whether the face image looked fearful or neutral. Keymapping was counterbalanced across participants, with half having left as neutral

and right as fearful, and the keys reversed for the other half of the sample. The task lasted four minutes. There were four runs collected, resulting in 384 total functional volumes. This included 72 face images presented each run (24 faces each for magno-biased, parvo-biased, and unbiased conditions) resulting in a total of 288 face images (96 faces each for magno-biased, parvo-biased, and unbiased conditions) and 96 null trials during with a fixation cross was presented in place of the face.

Neuroimaging Protocol

MRI images were collected using a 32-channel head coil on a 1.5 Tesla Siemens Avanto scanner. The scan parameters are as follows; 58 slices; TR = 2500 ms; TE = 33.83; flip angle = 90, FOV = 210 x 210, 3x3x2mm voxels, interleaved acquisition. Anatomical images were collected using a three-dimensional volume magnetization prepared rapid gradient echo (3D-MPRAGE) with 176 1mm, T1-weighted, straight sagittal slices (TR = 2300; TE = 2.28; flip angle = 8; FOV = 256).

Data Analysis

Region of Interest (ROI) Selection

To obtain the regions of interest (ROIs), structural MRI data was processed through FreeSurfer (https://surfer.nmr.mgh.harvard.edu/, version 6.0). FreeSurfer is an automated pipeline for anatomical segmentation and demarcation (Fischel, 2012). For this, subject-level data is first transformed into Talairach space and subsequently normalized for voxel intensity (Fischl et al., 2002). The program then divides and labels all subcortical regions using probabilistic segmentation estimated from a training data set provided in the package (Fischl et al., 2008). Following this, data is normalized for intensity a second time to separate white matter from everything else (Dale et al., 1999; Fischl et al., 1999). This separation is used as the template for creating a subject specific cortical surface. Once the surface is created and corrected for artifacts (e.g., a hole in a hemisphere that should not exist), the cortex is parcellated into different anatomical regions. This is based off both subject-specific information from the model (e.g., gyri

curvature, sulcal depth) and neuroanatomical landmarks derived from an atlas (Fischl & Dale, 2000; Desikan et al., 2006). Calculations of cortical and subcortical volumes using this method are comparable to manual segmentation (e.g., Lehmann et al., 2010). Because the visual pathways extend both dorsally and ventrally, each cortical region was included as an ROI. As for subcortical, only the amygdala and hippocampus were included due to previous work implicating their involvement in processing biased stimuli (Im et al., 2017; see Table 2).

Table 2: Regions of Interest for Magnocellular and Parvocellular Pathway

Regions of Interest (ROI)				
Frontal	*Parietal*	*Temporal*	*Occipital*	*Subcortical*
Caudal Anterior Cingulate^	Cuneus^	Entorhinal*	Lateral Occipital*^	Amygdala*
Caudal Middle Frontal^	Inferior Parietal^	Fusiform*	Pericalcarine*	Hippocampus*
Lateral Orbitofrontal^	Superior Parietal^	Inferior Temporal*	Precuneus^	
Medial Orbitofrontal^	Posterior Cingulate^	Middle Temporal*		
Pars Opercularis^		Parahippocampal*		
Pars Orbitalis^		Temporal Pole*		
Pars Triangularis^		Transverse Temporal*		
Super Frontal^		Superior Temporal*		

Note: Regions with ^ are dorsal brain regions, while those with * are ventral regions.

Functional Data Processing

The functional data was preprocessed using SPM12[2]. Each functional run was realigned to the mean image in each scan, corrected for motion and scanner artifacts using ArtRepair, and aligned to the MNI standard template (e.g., high-pass filtering) (Mazaika et al., 2009). The data were not spatially smoothed as this can negatively influence the results of classification (Mahmoudi et al., 2012). Finally, data was spatially normalized to standard space using the Montreal Neurological Institute (MNI) template implemented in SPM12. Images maintained the initial voxel resolution of 3x3x2mm. Importantly, all subsequent multi-voxel pattern analyses (MVPA) used non-normalized data for actual classification to prevent effects of smoothing and warping on classification.

Analysis Strategy Q1: Identification of Neural Specialization along Magnocellular/Parvocellular Pathway

To determine if neural patterns for magno-/parvo-specific stimuli can be distinguished along each visual pathway, I employed a MVPA approach to classify neural patterns within gray matter regions of the brain to test if patterns of the two types of stimuli are discernibly different, and whether this difference diminishes with age. To do this, trial-related activity was modeled in SPM12 using a general linear model (GLM) with a stick function corresponding to the trial onsets, convolved with a canonical hemodynamic response function. Each trial was modeled separately, resulting in individual beta maps for all trials of interest for each subject. An additional 6 nuisance regressors were included in each run corresponding to participant motion. Whole-brain beta parameter maps were generated for each trial for each run separately for each subject. In a given parameter map, the value in each voxel represents the regression coefficient for that trial's regressor in a multiple regression containing all other trials in the run and the motion parameters.

[2] Raw functional and structural data, including pre-calculated onset vectors, were provided by Dr. Kestutis Kveraga's lab on 2/5/19.

A linear discriminant analysis (LDA) was used to perform searchlight classification to determine if the pattern for magnocellular and parvocellular activation can be differentiated above chance (2 conditions; 50%). This process followed a standard leave-one-run-out cross-validation procedure where three runs of the functional data were used to train the classifier and one run was used to test the classifier accuracy. Voxel activation derived from the single trial model was used to test and train the classifier for each ROI separately (Table 2). To perform the searchlight, first a sphere with a radius of 6mm was centered on a single voxel. This serves as the test set of voxels for which to classify the two conditions. The resulting accuracy was then used as the value for the center voxel. The sphere then moved to the next voxel until all voxels with the ROI have been tested. The result of this procedure was a whole-ROI map of distinctiveness (accuracies) between conditions (see Carp et al., 2011a for a similar procedure). Following this, distinctiveness maps were normalized to MNI space using the ANTs toolbox (Tustison et al., 2014). Once maps were in a common space, maps for each region were entered into a whole-ROI one-sample t-test using FSL to determine clusters which exhibit statistical classification above chance (i.e., greater than 50% accuracy). Those clusters which were statistically above chance were then used as separate masks from which to pull activation magnitude (i.e., beta weights) for magno and parvo trials, separately, for each run.

Analysis Strategy Q2: Identification of Neural Specialization and Age-Related Dedifferentiation

To determine if there is age-related dedifferentiation to magno-/parvo-specific stimuli, I employed a MVPA approach to classify neural patterns within gray matter regions of the brain measure if these patterns diminish with age. To do this, I used the results of the previous MVPA classification analysis as my measure of neural pattern distinctiveness. Following the completion of the whole-ROI one-sample t-test, classification accuracies for each region were entered into a regression with age as the predictor. Regressions will be corrected for multiple comparisons using

a Bonferroni correction for 52 tests, corresponding to the 26 total regions across both hemisphere (26 x 2 = 52; 0.05/52 = 0.00096).

Q2 Sub-analyses

Analysis Strategy Q2A: Anterior-Posterior Differences in Dedifferentiation

An expansion on this analysis was done to examine the how the PASA theory of cognitive aging fits with the specialization of these pathways. The PASA theory is a well-known aging phenomenon characterized by over-recruitment of anterior brain areas to compensate for the under-recruitment of posterior regions (Davis et al., 2007; Cabeza & Dennis, 2012). To test this, I used the previous MVPA analyses from which to select the most anatomically anterior & posterior classification cluster. Next, I performed separate repeated measures ANOVA for magno- and parvo-specific regions, separately. The most anterior and posterior cluster for each pathway was entered into the ANOVA along will age as a covariate.

Analysis Strategy Q2B: Specialization and Dedifferentiation in Unbiased Faces

In another follow-up to Questions 1 & 2, in terms of biased stimuli, I also examined the comparison of magno/parvo stimuli to the unbiased stimuli. Given that the properties of these images would be detected by both pathways, it would make for an important comparison to understand the extent of magno/parvo specialization. To test this, I computed two additional searchlight analyses: one comparing parvo and unbiased stimuli, and another comparing magno and unbiased stimuli. In line with the previous MVPA pipeline (see Question 1: Identification of Neural Specialization), I identified areas of successful classification within the magno and parvo pathways, extracted beta weight activation, and compute t-tests to test for specialization. Additionally, I also tested for dedifferentiation by entering classification accuracy into a regression predicting age.

Analysis Strategy Q2C: Specialization and Dedifferentiation of Fear vs. Neutral Faces

In a final follow-up to Questions 1 & 2, I examined the comparison of face expression within these visual pathways. Previous work has suggested that expression information travels

along the magnocellular pathway to subcortical regions, and that accuracy in labeling expressions decreases in patients with dysfunction in this pathway (Vuilleumier & Pourtois, 2007; Bedwell et al., 2013). This can also be seen in multiple models of face processing, where emotion information is designated to dorsal pathways over ventral (Haxby et al., 2000; Gobbini & Haxby, 2007). However, greater activation to fearful faces compared to neutral has also been found in areas of the fusiform gyrus, driven by low spatial-frequency information (Vuilleumier & Pourtois, 2007). This would suggest that information beyond the visual specificity of the stimuli is being sent via these pathways. To test this, I computed two additional searchlight analyses: one comparing fearful and neutral parvo stimuli, and another comparing fearful and neutral magno stimuli. In line with the previous analysis pipeline (see Question 1: Identification of Neural Specialization), I identified areas of successful classification within the magno and parvo pathways and extracted activation weights for fearful and neutral for the condition-specific stimuli of the comparison (e.g., weights for parvo fearful and neutral in the parvo stimuli searchlight). Separate ANOVAs were computed for magno-/parvo-biased regions separately testing for specialization differences to the different types of threat. Additionally, I also tested for dedifferentiation by entering classification accuracy into a regression predicting age.

Analysis Strategy Q3: Neural Dedifferentiation and Threat Detection

To determine if age-related dedifferentiation of the magnocellular and parvocellular pathways impacts one's ability to detect threat in either or both visual pathways, I first used the behavioral data to determine if there was a relationship between ability to detect threat and age within this sample. While previous work has included age in analyses for behavioral accuracy for threat detection & participant, anxiety as well as whole brain sex differences for threat detection in these pathways, it was used as a covariate to control for rather than explicitly test the effect of the variable (Im et al., 2017, 2018). To explicitly assess the effect of age on threat detection accuracy, I created a mixed model ANOVA including expression (fear/neutral face), pathway

(magno/parvo), gaze (direct/averted) and behavioral accuracy, adding age as a regressor of interest to examine if and how age influences threat detection.

In order to test if dedifferentiation of the magnocellular and parvocellular pathways impacts one's ability to detect threat in either or both visual pathways, I employed a simple regression, using classification accuracies for magno/parvo stimuli within each region as the independent variable and behavioral accuracy for threat detection as the dependent variable.

Chapter 3

Results

Results: Specialization of Magnocellular and Parvocellular Pathway (Q1)

To determine if there is specialization to magno- or parvo-specific stimuli, I employed a MVPA searchlight analysis to classify the distinctiveness of neural patterns of magnocellular and parvocellular pathways. The results for each region were then submitted to separate one-sample t-tests to discern clusters of activation that could significantly discriminate between magno- and parvo-biased stimuli. The results of the foregoing t-tests revealed significant clusters of classification in the left fusiform gyrus, left pars opercularis, right hippocampus, right pars triangularis, and right superior frontal gyrus (p*s* < 0.05; Table 3). To further examine the specialization of these regions, beta weight activation for magno-biased and parvo-biased conditions were extracted from all significant clusters using SPM12. A paired-samples t-test contrasting beta weights from magno- and parvo biased conditions within each region[3] revealed no differences between stimuli conditions: left pars opercularis, $t(76) = 0.985$, $p = 0.328$, right pars triangularis, $t(76) = 0.883$, $p = 0.380$, right superior frontal, $t(76) = 0.089$, $p = 0.930$, and right hippocampus, $t(76) = -0.399$, $p = 0.691$ (Table 4). Together, results suggest that while neural activity in the foregoing clusters are distinguishable with respect to their responses to magno- and parvo- biased stimuli, there is no overall difference in the amount of neural activity evoked within each region. Importantly, while not statistically significant, frontal brain regions do show greater beta weight activation associated with magno-biased compared to parvo-biased stimuli, which is in line with the termination of the magno-pathway (Figure 4a-d). This relationship is reversed in the hippocampus, where parvo-biased activation is greater than magno-biased, and where the parvo-pathway innervates.

[3] Due to registration differences between packages, the beta weights could not be extracted for the left fusiform ROI.

Table 3: Group Searchlight Cluster Size

			Coordinates (MNI)			**Coordinates (TAL)**		
Hemisphere	**ROI**	**Cluster Size**	*X*	*Y*	*Z*	*X*	*Y*	*Z*
Left								
	Pars Opercularis	8	43	46	46	42	48	42
Right								
	Superior Frontal Gyrus	1	26	52	65	25	55	57
	Pars Triangularis	39	12	54	38	11	53	34
	Hippocampus	2	23	39	27	22	38	25

Table 4: Paired-Samples T-Test Between Magno-biased and Parvo-biased Beta Weights

		Magno/Parvo Selectivity		
Hemisphere	**ROI**	*df*	*t*	*p*
Left				
	Pars Opercularis	76	0.985	0.328
Right				
	Superior Frontal Gyrus	76	0.089	0.930
	Pars Triangularis	76	0.883	0.380
	Hippocampus	76	-0.399	0.691

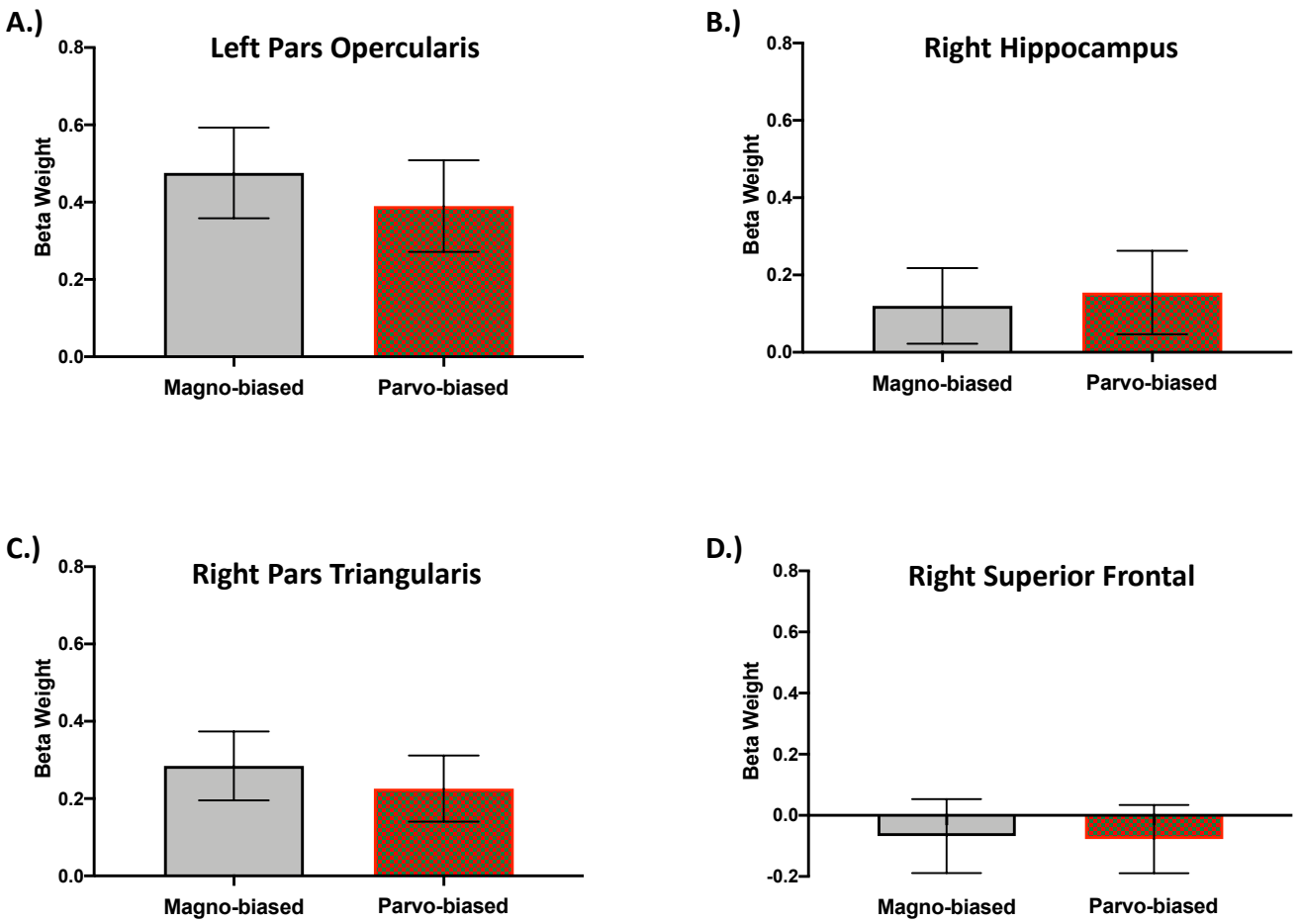

Figure 4. Beta Weight Activation from Magno-biased/Parvo-biased Searchlight Clusters

Results: Dedifferentiation of Magnocellular and Parvocellular Pathway (Q2)

In order to test for age-related dedifferentiation, overall cluster classification accuracy for each ROI was entered into a regression analysis predicting age separately. The rationale for performing this test in all regions is because regions that were not statistically different from chance at the group level could actually be driven by age-related effects in classification. The results revealed 2 negative relationships with age, one within the left pars orbitalis, $F(1, 76) = 8.890$, $r^2 = 0.106$, $p = 0.004$, and the other within the left inferior temporal gyrus, $F(1, 76) = 5.427$, $r^2 = 0.067$, $p = 0.023$ (Figure 5). In other words, for these two regions, decreases in classification accuracy were related to increases in subject age. However, these effects are not significant after Bonferroni correction (0.05/52 = 0.00096). There are no other relationships with age (see Table 3). Taken together, these results suggest that dedifferentiation does not occur within regions along the magnocellular and parvocellular pathways.

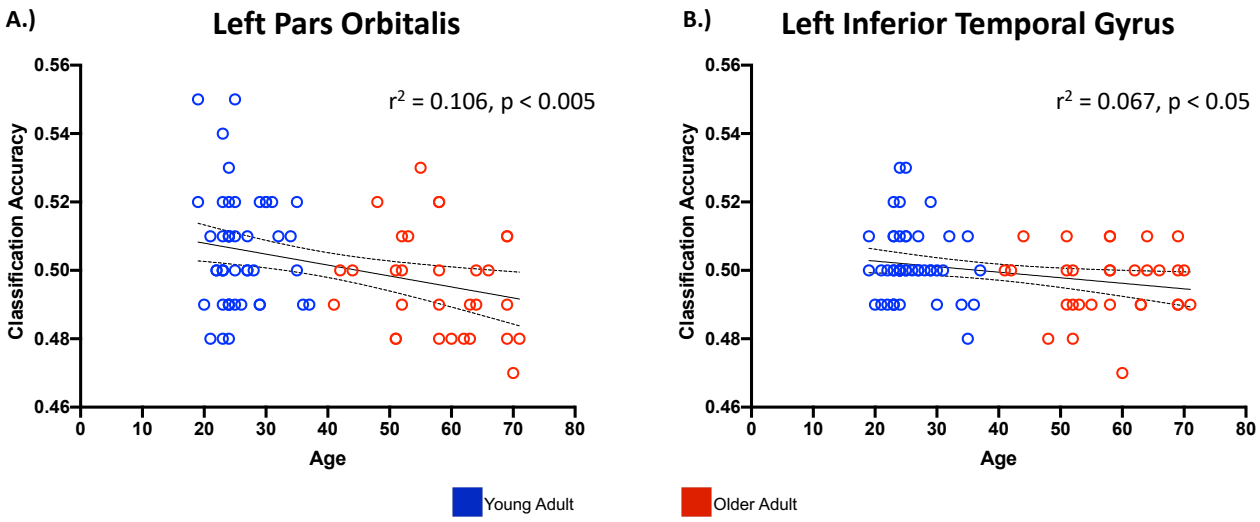

Figure 5. Regression of Classification Accuracy for Magno-biased/Parvo-biased Stimuli and Age

Results: Anterior-Posterior Differences in Dedifferentiation (Q2A)

In order to determine if there is age-related dedifferentiation related to PASA theory (i.e., greater dedifferentiation in anterior compared to posterior regions), classification accuracies for the most anterior and posterior clusters identified in the above analysis of magnocellular and parvocellular pathways were submitted to a repeated measures ANOVA. For the magnocellular pathway this included the left pars opercularis and right superior frontal gyrus. The results show no main effect of region, $F(2, 75) = 1.327$, $p = 0.253$, and no region x age interaction, $F(2, 75) = 1.893$, $p = 0.173$ (Table 5). Due to lack of significant results within the parvocellular pathway, there was only 1 region that showed significant classification that could be considered part of this pathway, which was the right hippocampus. Therefore, with only 1 region a repeated measures ANOVA could not be performed. However, as stated above, there is no effect of age on right hippocampus classification (see Table 6). As such, the results do not support the PASA theory given there was no dedifferentiation between anterior and posterior classification.

Table 5: Regressions with Searchlight Classification Accuracy for Mango/Parvo and Age

Left Hemisphere	**Age**			**Right Hemisphere**	**Age**		
ROI	*F*	*r2*	*p*		*F*	*r2*	*p*
Frontal							
Fontal Pole	2.830	0.041	0.097		0.031	0.000	0.861
Caudal Anterior Cingulate	0.031	0.000	0.861		1.682	0.022	0.199
Caudal Middle Frontal	0.141	0.002	0.708		3.086	0.040	0.083
Lateral Orbitofrontal	0.971	0.013	0.328		0.072	0.001	0.790
Medial Orbitofrontal	1.571	0.021	0.214		0.703	0.009	0.405
Pars Opercularis	0.578	0.008	0.450		0.734	0.010	0.394
Pars Orbitalis	**8.890**	**0.106**	**0.004**		0.682	0.009	0.412
Pars Triangularis	2.852	0.037	0.095		0.051	0.001	0.823
Superior Frontal	1.111	0.015	0.295		0.555	0.007	0.459
Parietal							
Cuneus	0.073	0.001	0.788		0.815	0.011	0.370
Inferior Parietal	0.169	0.002	0.682		2.513	0.032	0.117
Superior Parietal	0.452	0.006	0.504		0.742	0.010	0.392
Posterior Cingulate	0.058	0.001	0.810		0.272	0.004	0.604
Temporal							
Entorhinal	0.113	0.002	0.738		0.098	0.001	0.755
Fusiform	0.071	0.001	0.791		0.214	0.003	0.645
Inferior Temporal	**5.427**	**0.067**	**0.023**		0.034	0.000	0.854
Middle Temporal	1.861	0.024	0.177		0.110	0.001	0.741
Parahippocampal	3.429	0.044	0.068		0.582	0.008	0.448
Temporal Pole	0.209	0.003	0.649		0.368	0.005	0.546
Transverse Temporal	0.714	0.009	0.401		0.007	0.000	0.932
Superior Temporal	0.327	0.004	0.569		0.011	0.000	0.915
Occipital							
Lateral Occipital	1.148	0.015	0.288				
Pericalcarine	0.014	0.000	0.907		0.000	0.000	0.996
Precuneus	0.512	0.007	0.477		0.352	0.005	0.555
					0.052	0.001	0.820
Subcortical							
Amygdala	0.145	0.002	0.705		0.820	0.011	0.368
Hippocampus	3.758	0.048	0.056		0.227	0.003	0.635

Table 6: Repeated Measures ANOVA with Anterior/Posterior Magno-biased Regions and Age

	ANOVA Results			
	df	*F*	*p*	η^2
Magno	1, 75	1.327	0.250	0.017
Magno * Age	1, 75	1.893	0.173	0.025
Simple Effects				
R Sup Front = L Pars Operc			0.791	

Results: Dedifferentiation of Unbiased Faces (Q2B)

To test for discriminability differences along the magnocellular and parvocellular pathway for unbiased face stimuli (i.e, faces that are not magno- or parvo-biased), separate MVPA classification searchlight analyses were performed between (1) magno-biased and unbiased stimuli and (2) parvo-biased and unbiased stimuli in the same 54 regions noted above. As the unbiased stimuli have visual properties which would be detected by both pathways, this comparison can yield greater understanding in terms of the specialization for either or both visual pathways. The results for each region were then submitted to a one-sample t-test separately to discern clusters of activation within these regions that was statistically significantly above chance. For the magno/unbiased classification, a one-sample t-test revealed significant clusters of classification in the left parahippocampal gyrus (ps < 0.05; Table 7). For the parvo/unbiased classification, significant clusters were found in the left medial orbitofrontal ps < 0.05; Table 7) cortex and left transverse temporal gyrus (ps < 0.05; Table 7). Beta weight activation for visual pathway biased and unbiased conditions were extracted from all significant clusters using SPM12[4]. A paired-samples t-test contrasting beta weights from parvo-biased and unbiased conditions within the left transverse temporal gyrus revealed that unbiased stimuli elicited greater activation than parvo-biased stimuli, $t(76) = 2.672$, $p = 0.009$ (Figure 6).

[4] Due to registration differences between packages, the beta weights could not be extracted for the left parahippocampal and left medial orbitofrontal ROIs.

Table 7: Group Searchlight Cluster Size for Magno-Parvo-Unbiased Comparison

			Coordiantes (MNI)			**Coordiantes (TAL)**		
	ROI	**Cluster Size**	*X*	*Y*	*Z*	*X*	*Y*	*Z*
Magno vs. Unbiased								
Left Hemisphere								
	Parahippocampal Gyrus	1	39	33	24	-27	-27	-24
Parvo vs. Unbiased								
Left Hemisphere								
	Medial Orbitofrotnal Gyrus	106	-3	48	-28	-3	42	-28
	Transverse Temporal Gyrus	14	-45	-27	6	-43	-27	9

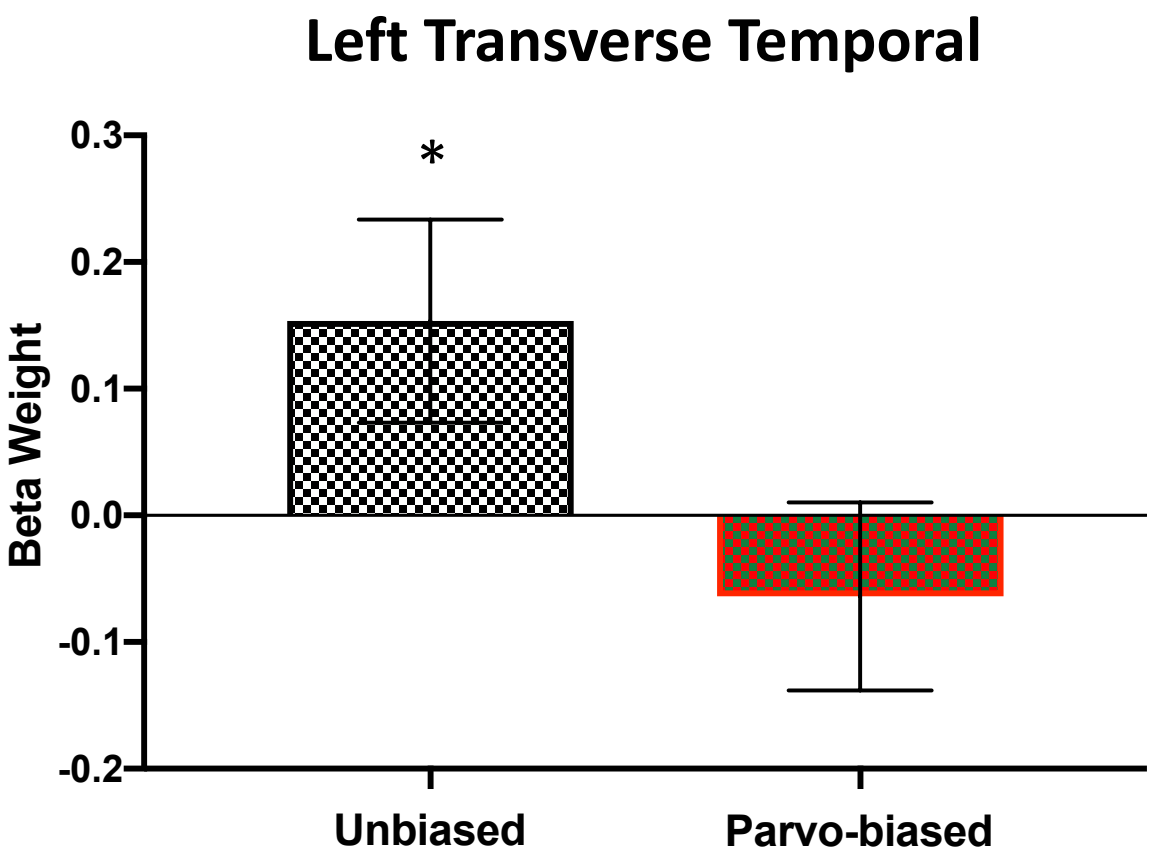

Figure 6. Beta Weight Activation from Unbiased/Parvo-biased Searchlight Clusters

In order to test for age-related dedifferentiation, overall cluster classification accuracy for each ROI for each classification (i.e., magno/unbiased, parvo/unbiased) was entered into a regression analysis predicting age separately. The rationale for performing this test in all regions is because regions that were not statistically different from chance at the group level could actually be driven by age-related effects in classification. For the magno/unbiased classification the results revealed a positive relationship with age and the right parahippocampal gyrus $F(1, 76) = 4.681$, $r^2 = 0.059$, $p = 0.034$ (Figure 7a). For the parvo/unbiased classification the results revealed a negative relationship with age and the left amygdala, $F(1, 75) = 6.660$, $r^2 = 0.083$, $p = 0.012$ (Figure 7b), but also 3 positive relationships between age and the left caudal anterior cingulate, $F(1, 76) = 5.997$, $r^2 = 0.074$, $p = 0.017$ (Figure 7c), the left parahippocampal gyrus, $F(1, 76) = 4.389$, $r^2 = 0.055$, $p = 0.040$ (Figure 7d), and the right precuneus, $F(1, 76) = 4.050$, $r^2 = 0.051$, $p = 0.048$ (Figure 7e). However, these effects are not significant after Bonferroni correction (0.05/52 = 0.00096). There are no other relationships with age and magno/unbiased (Table 8) or parvo/unbiased (Table 9). Taken together, these results suggest that dedifferentiation for unbiased stimuli does not occur within regions along the magnocellular and parvocellular pathways.

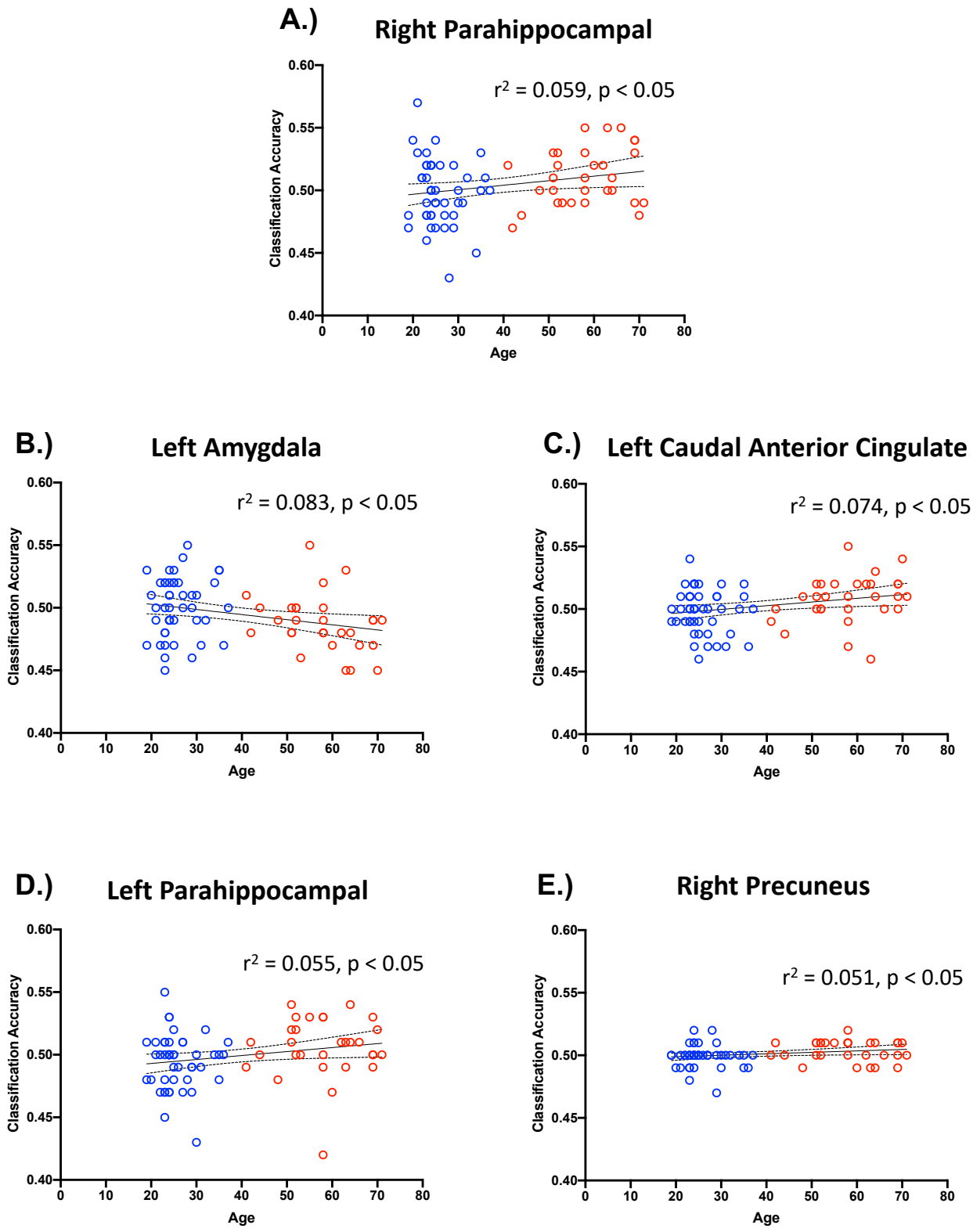

Figure 7. Regression of Classification Accuracy for Magno-biased/Parvo-biased/Unbiased Stimuli and Age

Table 8: Regressions with Searchlight Classification Accuracy for Magno/Unbiased and Age

Left Hemisphere	**Age**			**Right Hemisphere**	**Age**		
ROI	*F*	*r2*	*p*		*F*	*r2*	*p*
Frontal							
Fontal Pole	0.408	0.006	0.525		3.706	0.048	0.058
Caudal Anterior Cingulate	1.394	0.018	0.242		3.791	0.048	0.055
Caudal Middle Frontal	2.317	0.030	0.132		0.014	0.000	0.907
Lateral Orbitofrontal	0.706	0.009	0.403		0.113	0.002	0.737
Medial Orbitofrontal	1.557	0.020	0.216		0.683	0.009	0.411
Pars Opercularis	0.807	0.011	0.372		0.080	0.001	0.778
Pars Orbitalis	0.347	0.005	0.558		0.069	0.001	0.794
Pars Triangularis	0.140	0.002	0.710		0.660	0.009	0.419
Super Frontal	0.001	0.000	0.969		0.000	0.000	0.996
Parietal							
Cuneus	0.085	0.001	0.771		0.014	0.000	0.907
Inferior Parietal	1.053	0.014	0.308		2.758	0.035	0.101
Superior Parietal	0.960	0.013	0.330		0.747	0.010	0.390
Posterior Cingulate	0.203	0.003	0.654		2.183	0.028	0.144
Temporal							
Entorhinal	0.195	0.003	0.660		0.018	0.000	0.894
Fusiform	0.347	0.005	0.558		0.037	0.000	0.848
Inferior Temporal	0.007	0.000	0.932		2.246	0.029	0.138
Middle Temporal	0.357	0.005	0.552		0.028	0.000	0.868
Parahippocampal	0.061	0.001	0.805		**4.681**	**0.059**	**0.034**
Temporal Pole	0.027	0.000	0.870		1.157	0.015	0.286
Transverse Temporal	1.754	0.023	0.189		0.410	0.006	0.524
Superior Temporal	0.003	0.000	0.956		0.414	0.005	0.522
Occipital							
Lateral Occipital	0.732	0.010	0.395		0.016	0.000	0.901
Pericalcarine	0.006	0.000	0.939		1.441	0.019	0.234
Precuneus	1.232	0.016	0.271		1.734	0.023	0.192
Subcortical							
Amygdala	0.694	0.009	0.407		0.111	0.001	0.740
Hippocampus	0.455	0.006	0.502		2.004	0.026	0.161

Table 9: Regressions with Searchlight Classification Accuracy for Parvo/Unbiased and Age

Left Hemisphere	**Age**			**Right Hemisphere**	**Age**		
ROI	*F*	*r2*	*p*		*F*	*r2*	*p*
Frontal							
Fontal Pole	1.666	0.024	0.201		0.179	0.002	0.674
Caudal Anterior Cingulate	**5.997**	**0.074**	**0.017**		0.794	0.010	0.376
Caudal Middle Frontal	0.040	0.001	0.843		0.345	0.005	0.559
Lateral Orbitofrontal	2.513	0.032	0.117		0.015	0.000	0.904
Medial Orbitofrontal	0.455	0.006	0.502		2.215	0.029	0.141
Pars Opercularis	0.116	0.002	0.735		0.001	0.000	0.975
Pars Orbitalis	1.250	0.016	0.267		0.266	0.004	0.607
Pars Triangularis	0.886	0.012	0.350		0.005	0.000	0.945
Super Frontal	0.035	0.000	0.851		0.099	0.001	0.754
Parietal							
Cuneus	0.065	0.001	0.799		0.253	0.003	0.616
Inferior Parietal	0.844	0.011	0.361		0.006	0.000	0.938
Superior Parietal	0.632	0.008	0.429		1.151	0.015	0.287
Posterior Cingulate	0.050	0.001	0.824		0.127	0.002	0.723
Temporal							
Entorhinal	0.094	0.001	0.760		0.368	0.005	0.546
Fusiform	0.279	0.004	0.599		0.772	0.010	0.382
Inferior Temporal	0.420	0.006	0.519		0.212	0.003	0.647
Middle Temporal	0.036	0.000	0.850		0.004	0.000	0.952
Parahippocampal	**4.389**	**0.055**	**0.040**		0.603	0.008	0.440
Temporal Pole	0.001	0.000	0.976		0.240	0.003	0.626
Transverse Temporal	2.828	0.036	0.097		2.510	0.034	0.118
Superior Temporal	0.384	0.005	0.537		2.431	0.031	0.123
Occipital							
Lateral Occipital	1.667	0.022	0.201		0.560	0.007	0.457
Pericalcarine	0.444	0.006	0.507		0.760	0.010	0.386
Precuneus	1.314	0.017	0.255		**4.050**	**0.051**	**0.048**
Subcortical							
Amygdala	**6.660**	**0.083**	**0.012**		0.059	0.001	0.808
Hippocampus	0.096	0.001	0.758		0.716	0.009	0.400

Results: Dedifferentiation of Fear vs. Neutral Faces (Q2C)

Finally, I sought to test for discriminability differences along the magnocellular and parvocellular pathway for face expression. For this, I computed two additional searchlight analyses: one comparing fearful and neutral parvo stimuli, and another comparing fearful and neutral magno stimuli. For the magno-biased stimuli classification, a one-sample t-test revealed significant clusters of classification for face emotionality in the left entorhinal gyrus (ps < 0.05), right amygdala (ps < 0.05), and right frontal pole (ps < 0.05; Table 10). Additionally, for the parvo-biased classification, significant clusters were found in the left hippocampus and right cuneus (ps < 0.05; Table 10). A paired-samples t-test contrasting beta weights for fearful and neutral faces within visual biased condition within each region[5] revealed that there is no difference between conditions for the right amygdala t(76) = 1.791, p = 0.077, or the right cuneus t(76) = 0.004, p = 0.997 (Figure 8).

[5] Due to registration differences between packages, the beta weights could not be extracted for the left entorhinal, right frontal pole, and left hippocampus ROIs.

Table 10: Group Searchlight Cluster Size for Fear-Neutral Comparison

			Coordinates (MNI)			**Coordinates (TAL)**		
	ROI	**Cluster Size**	*X*	*Y*	*Z*	*X*	*Y*	*Z*
Magno-biased								
Left Hemisphere								
	Entorhinal Cortex	17	-21	-15	-38	-20	-17	-29
		2	-24	-3	-38	-24	-6	-30
		1	-18	-12	-26	-17	-14	-18
Right Hemisphere								
	Frontal Pole	27	12	66	-14	11	60	-15
		12	6	69	-6	5	63	-6
		6	3	60	-18	2	53	-19
	Amygdala	1	24	-3	-32	23	-6	-24
		1	24	-9	-22	23	-11	-15
Parvo-biased								
Left Hemisphere								
	Hippocampus	1	-27	-18	-12	-26	-19	-6
Right Hemisphere								
	Cuneus	1	12	-63	12	12	-61	14
		1	15	-69	14	15	-67	16

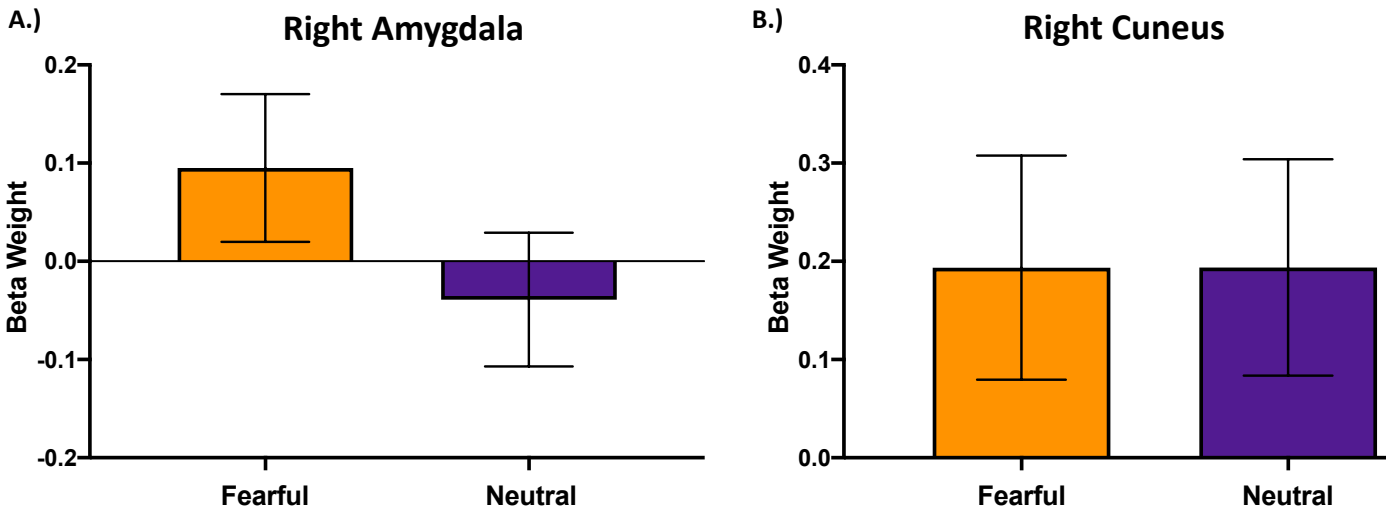

Figure 8. Beta Weight Activation from Visually Biased Fearful/Neutral Searchlight Clusters

In order to test for age-related dedifferentiation, overall cluster classification accuracy for each ROI for each classification (i.e., magno-biased fear/neutral, parvo-biased fear/neutral) was entered into a regression analysis predicting age separately. The rationale for performing this test in all regions is because regions that were not statistically different from chance at the group level could actually be driven by age-related effects in classification. For the magno-biased classification for fearful/neutral faces, the results revealed a positive relationship with age and the left amygdala $F(1, 75) = 5.023$, $r^2 = 0.064$, $p = 0.028$ (Figure 9). There are no other relationships for magno-biased stimuli (Table 11). For the parvo-biased classification for fearful/neutral faces, there were no relationships with age (Table 12). However, these effects are not significant after Bonferroni correction (0.05/52 = 0.00096). Taken together, these results suggest that dedifferentiation for unbiased stimuli does not occur within regions along the magnocellular and parvocellular pathways. Overall, this suggests that neural patterns of facial expression are discriminable within regions along both visual pathways, especially in subcortical and temporal regions associated with processing of faces and emotion (Kanwisher al., 1997; Habel et al., 2007; Elbich & Scherf, 2017), and show no effects of dedifferentiation.

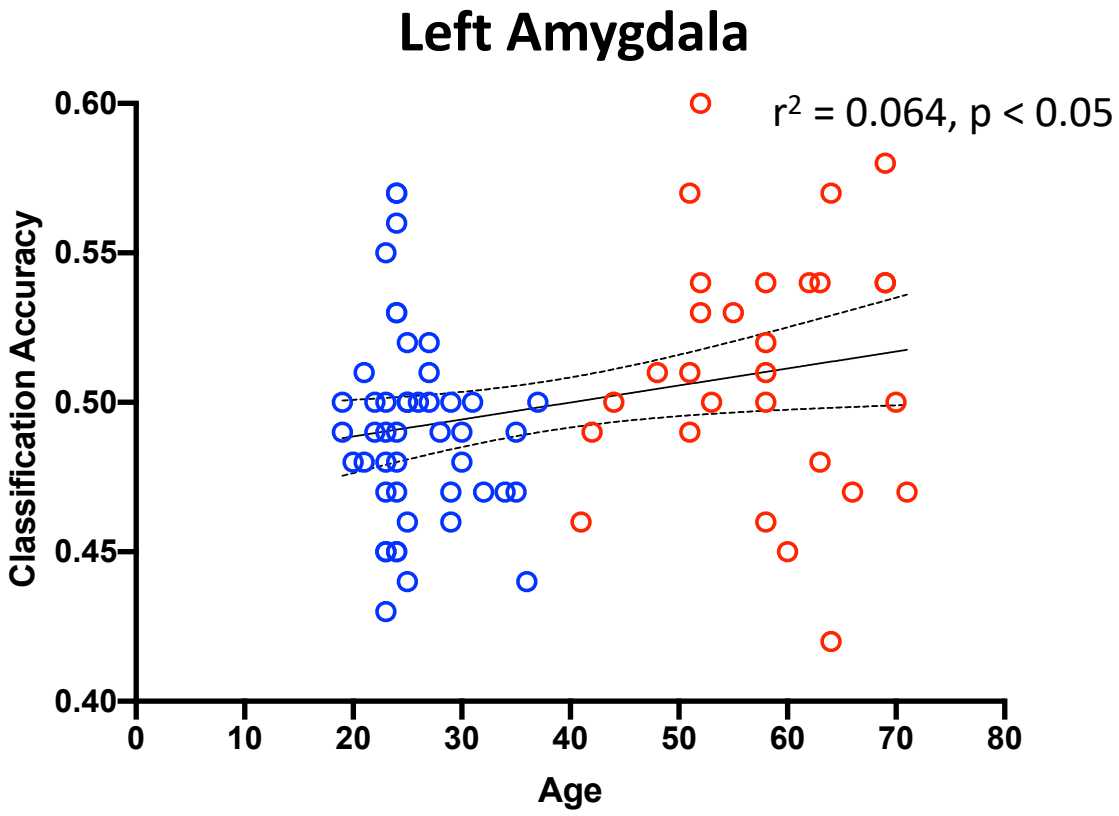

Figure 9. Regression of Classification Accuracy for Visually Biased Fearful/Neutral Stimuli and Age

Table 11: Regressions with Searchlight Classification Accuracy for Magno-biased Fear/Neutral and Age

Left Hemisphere	**Age**			**Right Hemisphere**	**Age**		
ROI	*F*	*r2*	*p*		*F*	*r2*	*p*
Frontal							
Fontal Pole	1.364	0.020	0.247		0.911	0.012	0.343
Caudal Anterior Cingulate	0.000	0.000	0.988		0.647	0.009	0.424
Caudal Middle Frontal	0.072	0.001	0.789		0.299	0.004	0.586
Lateral Orbitofrontal	0.331	0.004	0.567		0.357	0.005	0.552
Medial Orbitofrontal	0.127	0.002	0.723		0.951	0.013	0.333
Pars Opercularis	0.804	0.011	0.373		0.433	0.006	0.513
Pars Orbitalis	0.167	0.002	0.684		0.063	0.001	0.803
Pars Triangularis	0.001	0.000	0.979		2.097	0.027	0.152
Super Frontal	1.303	0.017	0.257		0.018	0.000	0.893
Parietal							
Cuneus	1.891	0.025	0.173		0.093	0.001	0.761
Inferior Parietal	0.018	0.000	0.894		0.668	0.009	0.416
Superior Parietal	1.222	0.016	0.272		0.390	0.005	0.534
Posterior Cingulate	1.696	0.022	0.197		1.612	0.021	0.208
Temporal							
Entorhinal	0.317	0.004	0.575		0.017	0.000	0.897
Fusiform	0.174	0.002	0.678		0.114	0.002	0.736
Inferior Temporal	0.969	0.013	0.328		0.608	0.008	0.438
Middle Temporal	0.091	0.001	0.764		1.050	0.014	0.309
Parahippocampal	2.520	0.033	0.117		3.297	0.042	0.073
Temporal Pole	0.048	0.001	0.828		0.226	0.003	0.636
Transverse Temporal	1.318	0.017	0.255		1.264	0.018	0.265
Superior Temporal	1.221	0.016	0.273		0.049	0.001	0.826
Occipital							
Lateral Occipital	0.111	0.001	0.740		0.899	0.012	0.346
Pericalcarine	0.003	0.000	0.960		1.385	0.018	0.243
Precuneus	0.112	0.001	0.739		0.034	0.000	0.854
Subcortical							
Amygdala	**5.023**	**0.064**	**0.028**		0.621	0.008	0.433
Hippocampus	1.753	0.023	0.190		3.117	0.040	0.082

Table 12: Regressions with Searchlight Classification Accuracy for Parvo-biased Fear/Neutral and Age

Left Hemisphere	**Age**			**Right Hemisphere**	**Age**		
ROI	*F*	*r2*	*p*		*F*	*r2*	*p*
Frontal							
Fontal Pole	3.700	0.052	0.059		0.099	0.001	0.754
Caudal Anterior Cingulate	0.826	0.011	0.366		3.157	0.041	0.080
Caudal Middle Frontal	0.012	0.000	0.914		0.314	0.004	0.577
Lateral Orbitofrontal	0.016	0.000	0.898		0.004	0.000	0.949
Medial Orbitofrontal	2.815	0.037	0.098		1.094	0.015	0.299
Pars Opercularis	1.752	0.023	0.190		1.847	0.024	0.178
Pars Orbitalis	0.547	0.007	0.462		2.249	0.029	0.138
Pars Triangularis	1.761	0.023	0.189		0.618	0.008	0.434
Super Frontal	0.548	0.007	0.461		0.000	0.000	0.999
Parietal							
Cuneus	0.024	0.000	0.877		0.042	0.001	0.839
Inferior Parietal	1.187	0.016	0.280		0.012	0.000	0.911
Superior Parietal	0.603	0.008	0.440		0.095	0.001	0.758
Posterior Cingulate	0.019	0.000	0.891		2.835	0.037	0.096
Temporal							
Entorhinal	0.068	0.001	0.795		0.003	0.000	0.958
Fusiform	0.215	0.003	0.644		1.175	0.016	0.282
Inferior Temporal	0.295	0.004	0.589		0.000	0.000	0.994
Middle Temporal	0.000	0.000	0.988		1.373	0.018	0.245
Parahippocampal	0.710	0.010	0.402		0.145	0.002	0.704
Temporal Pole	0.268	0.004	0.606		0.011	0.000	0.916
Transverse Temporal	0.042	0.001	0.839		1.741	0.024	0.191
Superior Temporal	0.112	0.002	0.739		0.160	0.002	0.690
Occipital							
Lateral Occipital	1.207	0.016	0.276		1.011	0.013	0.318
Pericalcarine	0.504	0.007	0.480		0.082	0.001	0.776
Precuneus	0.103	0.001	0.749		0.017	0.000	0.897
Subcortical							
Amygdala	0.102	0.001	0.750		0.233	0.003	0.631
Hippocampus	0.004	0.000	0.948		0.000	0.000	0.983

Results: Neural Dedifferentiation and Threat Detection (Q3)

To determine if age-related dedifferentiation of the magnocellular and parvocellular pathways impacts one's ability to detect threat in either or both visual pathways, I created a mixed model ANOVA including expression (fear/neutral face), pathway (magno/parvo), gaze (direct/averted) and behavioral accuracy, with age as a covariate of interest. The results show a main effect of behavioral accuracy both expression, $F(1, 75) = 5.321$, $p = 0.024$, and gaze, $F(1, 75) = 5.164$, $p = 0.026$, but not of pathway, $F(1, 75) = 2.953$, $p = 0.090$ (Table 13). Simple effects test reveal that overall neutral faces (M = 92.52) had greater accuracy than fearful faces (M = 87.88) ($p < 0.001$). In addition, in terms of gaze direction, directed gaze faces (M = 91.07) had greater accuracy than averted gaze faces (M = 89.32) ($p < 0.001$). There were no significant interactions with any metric or interactions with age (Table 13).

In order to test if dedifferentiation of the magnocellular and parvocellular pathways impacts one's ability to detect threat in either or both visual pathways, classification accuracies for magno- and parvo-biased stimuli within each region were entered into a regression with behavioral accuracy for threat detection as the dependent variable. The results show multiple effects of clear and ambiguous threat in both frontal cortex and subcortical regions (Tables 14-17). Classification accuracy for the left pars orbitalis shows a negative relationship with behavioral accuracy for both magno-biased averted fear faces, $F(1, 76) = 9.310$, $r^2 = 0.110$, $p = 0.003$ (Table 14; Figure 10a), and parvo-biased directed fear faces, $F(1, 76) = 4.979$, $r^2 = 0.062$, $p = 0.029$ (Table 15; Figure 10b). Additionally, classification accuracy in right amygdala exhibits a negative relationship with magno-biased averted fear faces, $F(1, 76) = 7.036$, $r^2 = 0.086$, $p = 0.010$ (Table 14; Figure 11). Finally, in the right hippocampus, classification accuracy again has a negative relationship with both magno-biased directed fear, $F(1, 76) = 4.856$, $r^2 = 0.061$, $p = 0.031$ (Table 16; Figure 12a), and magno-biased averted fear faces, $F(1, 76) = 4.822$, $r^2 = 0.060$, $p = 0.031$(Table 14; Figure 12b). However, these effects are not significant after Bonferroni

correction (0.05/52 = 0.00096). Taken together, these results show there is no relationship between dedifferentiation of either visual pathway and the ability to detect facial threat.

Table 13: Repeated-Measures ANOVA with Behavioral Task Accuracy

	Repeated Measures			
Comparison	**df**	*F*	*p*	*eta2*
Expression	**1, 75**	**5.321**	**0.024**	**0.066**
Expression * Age	1, 75	0.000	0.992	0.000
Pathway	1, 75	2.953	0.090	0.038
Pathway * Age	1, 75	0.083	0.773	0.001
Gaze	**1, 75**	**5.164**	**0.026**	**0.064**
Gaze * Age	1, 75	0.417	0.520	0.006
Expression * Pathway	1, 75	0.388	0.535	0.005
Expression * Pathway * Age	1, 75	1.040	0.311	0.014
Pathway * Gaze	1, 75	1.584	0.212	0.021
Pathway * Gaze * Age	1, 75	0.792	0.376	0.010
Gaze * Expression	1, 75	2.179	0.144	0.028
Gaze * Expression * Age	1, 75	0.034	0.854	0.000
Expression * Pathway * Gaze	1, 75	0.735	0.394	0.010
Expression * Pathway * Gaze * Age	1, 75	1.204	0.276	0.016
Main Effects Pairwise Comparison				
Expression				
Neutral > Fear			**<0.001**	
Gaze				
Averted > Direct			**<0.001**	

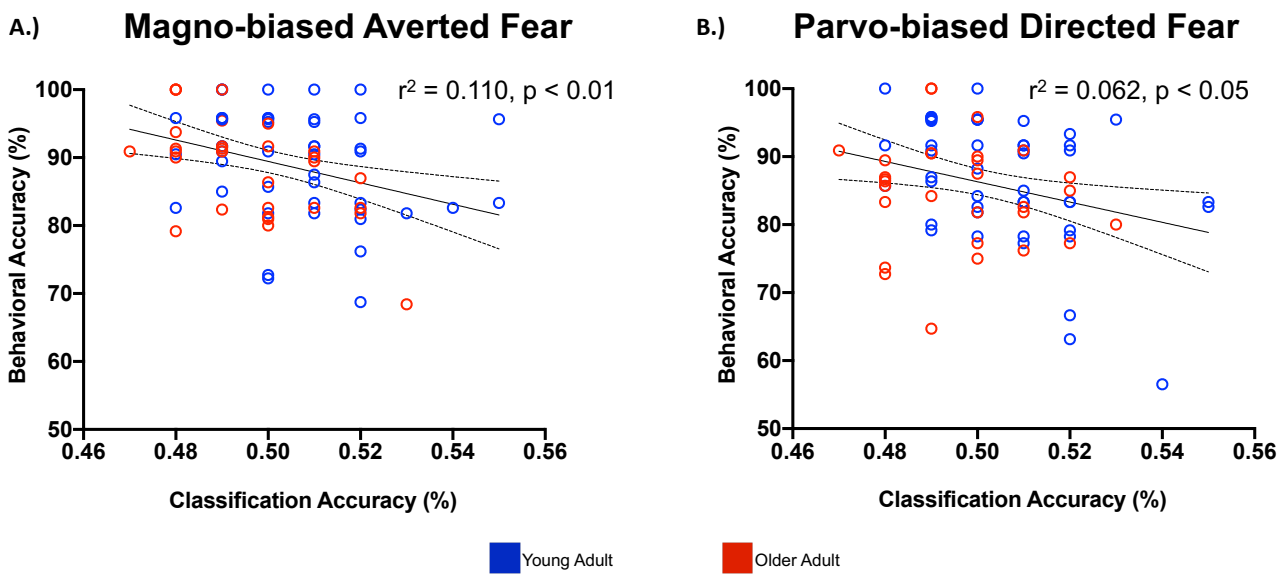

Figure 10. Regression with Classification Accuracy for Magno-biased/Parvo-biased Stimuli and Behavioral Accuracy for Magno-biased/Parvo-biased Threat Stimuli

Table 14: Regressions with Searchlight Classification Accuracy for Magno/Parvo-biased Stimuli and Behavioral Accuracy for Magno-biased Ambiguous Threat

Left Hemisphere	**Age**			**Right Hemisphere**	**Age**		
ROI	*F*	*r2*	*p*		*F*	*r2*	*p*
Frontal							
Fontal Pole	3.155	0.045	0.080		1.469	0.019	0.229
Caudal Anterior Cingulate	0.184	0.002	0.670		2.980	0.038	0.088
Caudal Middle Frontal	0.539	0.007	0.465		0.697	0.009	0.406
Lateral Orbitofrontal	0.281	0.004	0.598		0.074	0.001	0.786
Medial Orbitofrontal	0.018	0.000	0.893		0.683	0.009	0.411
Pars Opercularis	0.043	0.001	0.836		1.811	0.024	0.182
Pars Orbitalis	0.135	0.002	0.715		0.042	0.001	0.839
Pars Triangularis	1.203	0.016	0.276		2.307	0.030	0.133
Super Frontal	0.584	0.008	0.447		0.000	0.000	0.990
Parietal							
Cuneus	0.776	0.010	0.381		1.745	0.023	0.191
Inferior Parietal	0.117	0.002	0.733		2.946	0.038	0.090
Superior Parietal	2.308	0.030	0.133		0.165	0.002	0.686
Posterior Cingulate	0.076	0.001	0.784		1.317	0.017	0.255
Temporal							
Entorhinal	0.127	0.002	0.723		0.097	0.001	0.756
Fusiform	0.537	0.007	0.466		0.250	0.003	0.618
Inferior Temporal	0.731	0.010	0.395		1.230	0.016	0.271
Middle Temporal	0.018	0.000	0.895		0.511	0.007	0.477
Parahippocampal	0.108	0.001	0.743		0.066	0.001	0.798
Temporal Pole	0.009	0.000	0.923		0.124	0.002	0.725
Transverse Temporal	0.202	0.003	0.654		0.361	0.005	0.550
Superior Temporal	0.114	0.002	0.737		0.361	0.005	0.550
Occipital							
Lateral Occipital	0.083	0.001	0.774		0.049	0.001	0.825
Pericalcarine	0.920	0.012	0.341		0.072	0.001	0.789
Precuneus	0.536	0.007	0.466		0.428	0.006	0.515
Subcortical							
Amygdala	0.007	0.000	0.932		0.015	0.000	0.903
Hippocampus	3.269	0.042	0.075		**4.856**	**0.061**	**0.031**

Table 15: Regressions with Searchlight Classification Accuracy for Magno/Parvo-biased Stimuli and Behavioral Accuracy for Magno-biased Direct Threat

Left Hemisphere	**Age**			**Right Hemisphere**	**Age**		
ROI	*F*	*r2*	*p*		*F*	*r2*	*p*
Frontal							
Fontal Pole	0.001	0.000	0.970		2.882	0.037	0.094
Caudal Anterior Cingulate	0.599	0.008	0.441		0.001	0.000	0.981
Caudal Middle Frontal	0.260	0.003	0.612		0.205	0.003	0.652
Lateral Orbitofrontal	0.011	0.000	0.917		0.051	0.001	0.822
Medial Orbitofrontal	0.603	0.008	0.440		0.240	0.003	0.626
Pars Opercularis	0.003	0.000	0.959		1.297	0.017	0.258
Pars Orbitalis	**9.310**	**0.110**	**0.003**		0.272	0.004	0.603
Pars Triangularis	0.973	0.013	0.327		0.029	0.000	0.866
Super Frontal	0.864	0.011	0.356		0.022	0.000	0.883
Parietal							
Cuneus	0.769	0.010	0.383		0.481	0.006	0.490
Inferior Parietal	0.019	0.000	0.890		0.137	0.002	0.713
Superior Parietal	2.079	0.027	0.153		3.643	0.046	0.060
Posterior Cingulate	0.373	0.005	0.543		0.990	0.013	0.323
Temporal							
Entorhinal	0.028	0.000	0.868		0.585	0.008	0.447
Fusiform	0.007	0.000	0.932		0.446	0.006	0.506
Inferior Temporal	0.341	0.005	0.561		0.014	0.000	0.905
Middle Temporal	0.175	0.002	0.677		3.606	0.046	0.061
Parahippocampal	3.463	0.044	0.067		2.731	0.035	0.103
Temporal Pole	0.587	0.008	0.446		0.804	0.011	0.373
Transverse Temporal	3.037	0.039	0.085		2.018	0.028	0.160
Superior Temporal	0.079	0.001	0.779		0.191	0.003	0.664
Occipital							
Lateral Occipital	0.552	0.007	0.460		1.719	0.022	0.194
Pericalcarine	2.444	0.032	0.122		0.469	0.006	0.496
Precuneus	0.809	0.011	0.371		1.512	0.020	0.223
Subcortical							
Amygdala	2.595	0.034	0.111		**7.036**	**0.086**	**0.010**
Hippocampus	0.000	0.000	0.993		**4.822**	**0.060**	**0.031**

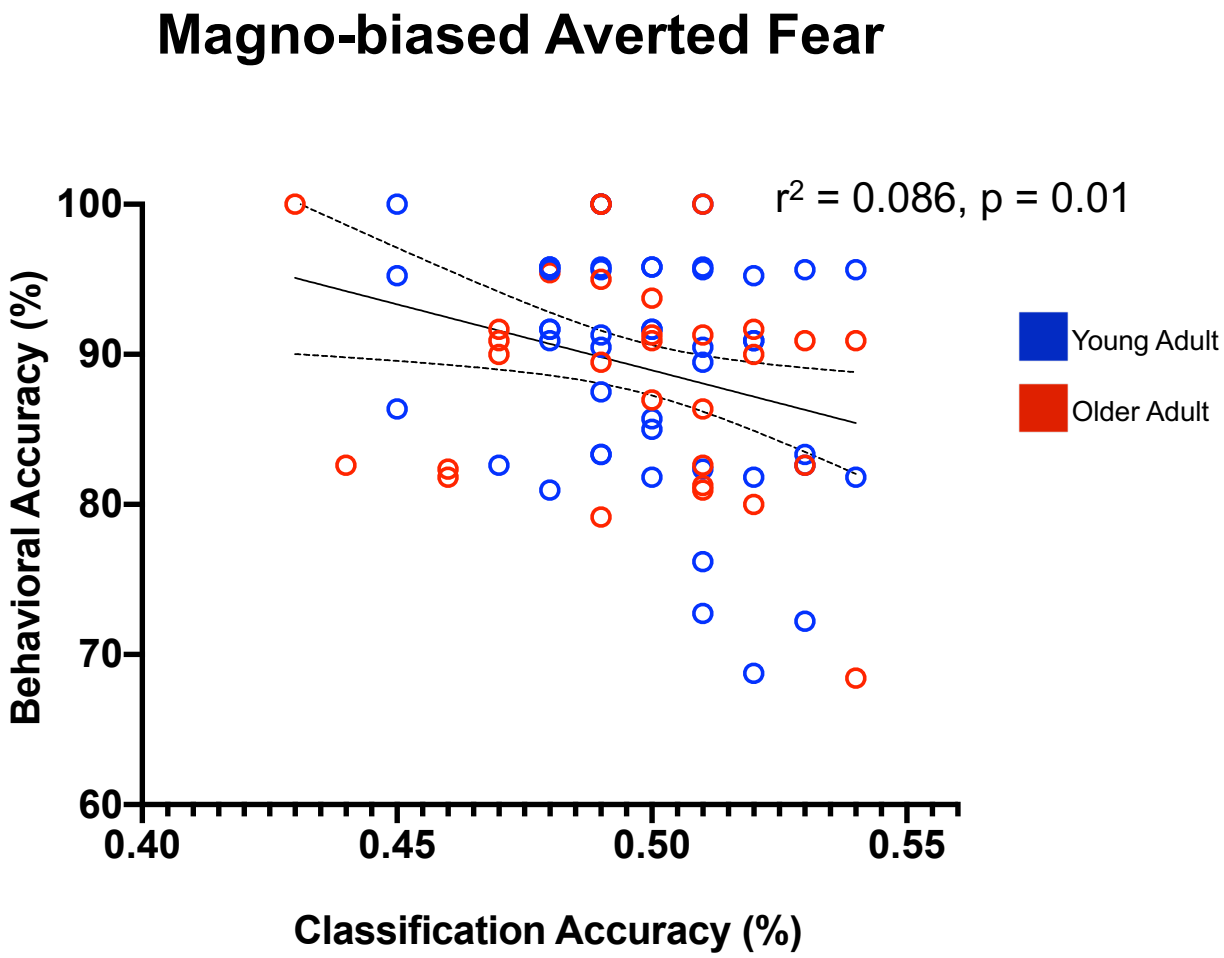

Figure 11. Regression with Classification Accuracy for Magno-biased/Parvo-biased Stimuli and Behavioral Accuracy for Magno-biased Clear Threat Stimuli

Table 16: Regressions with Searchlight Classification Accuracy for Magno/Parvo-biased Stimuli and Behavioral Accuracy for Parvo-biased Ambiguous Threat

Left Hemisphere	**Age**			**Right Hemisphere**	**Age**		
ROI	*F*	*r2*	*p*		*F*	*r2*	*p*
Frontal							
Fontal Pole	2.291	0.033	0.135		0.170	0.002	0.681
Caudal Anterior Cingulate	0.519	0.007	0.473		1.415	0.019	0.238
Caudal Middle Frontal	0.183	0.002	0.670		0.423	0.006	0.517
Lateral Orbitofrontal	2.182	0.028	0.144		0.089	0.001	0.766
Medial Orbitofrontal	0.002	0.000	0.968		0.027	0.000	0.869
Pars Opercularis	0.013	0.000	0.908		0.002	0.000	0.963
Pars Orbitalis	**4.979**	**0.062**	**0.029**		0.091	0.001	0.764
Pars Triangularis	1.778	0.023	0.186		0.061	0.001	0.806
Super Frontal	0.043	0.001	0.837		2.853	0.037	0.095
Parietal							
Cuneus	0.723	0.010	0.398		3.371	0.043	0.070
Inferior Parietal	0.194	0.003	0.661		0.532	0.007	0.468
Superior Parietal	0.036	0.000	0.851		0.150	0.002	0.700
Posterior Cingulate	0.154	0.002	0.696		2.199	0.028	0.142
Temporal							
Entorhinal	3.356	0.043	0.071		0.028	0.000	0.868
Fusiform	0.317	0.004	0.575		0.699	0.009	0.406
Inferior Temporal	0.071	0.001	0.790		0.691	0.009	0.408
Middle Temporal	0.063	0.001	0.802		0.740	0.010	0.392
Parahippocampal	0.068	0.001	0.795		0.836	0.011	0.364
Temporal Pole	0.120	0.002	0.730		0.716	0.010	0.400
Transverse Temporal	0.518	0.007	0.474		0.586	0.008	0.446
Superior Temporal	0.574	0.008	0.451		1.819	0.024	0.181
Occipital							
Lateral Occipital	0.005	0.000	0.942		0.429	0.006	0.515
Pericalcarine	0.109	0.001	0.742		1.054	0.014	0.308
Precuneus	0.012	0.000	0.913		0.174	0.002	0.678
Subcortical							
Amygdala	0.019	0.000	0.891		1.047	0.014	0.310
Hippocampus	3.461	0.044	0.067		0.042	0.001	0.838

Table 17: Regressions with Searchlight Classification Accuracy for Magno/Parvo-biased Stimuli and Behavioral Accuracy for Parvo-biased Direct Threat

Left Hemisphere	**Age**			**Right Hemisphere**	**Age**		
ROI	*F*	*r2*	*p*		*F*	*r2*	*p*
Frontal							
Fontal Pole	0.562	0.008	0.456		1.273	0.017	0.263
Caudal Anterior Cingulate	0.010	0.000	0.921		0.156	0.002	0.694
Caudal Middle Frontal	0.967	0.013	0.329		0.830	0.011	0.365
Lateral Orbitofrontal	0.753	0.010	0.388		0.446	0.006	0.506
Medial Orbitofrontal	0.008	0.000	0.928		0.076	0.001	0.784
Pars Opercularis	2.383	0.031	0.127		0.270	0.004	0.605
Pars Orbitalis	0.241	0.003	0.625		0.836	0.011	0.363
Pars Triangularis	0.608	0.008	0.438		0.064	0.001	0.801
Super Frontal	0.032	0.000	0.857		0.157	0.002	0.693
					0.928	0.012	0.339
Parietal							
Cuneus	0.179	0.002	0.674		0.006	0.000	0.936
Inferior Parietal	0.841	0.011	0.362		0.938	0.012	0.336
Superior Parietal	2.787	0.036	0.099				
Posterior Cingulate	0.359	0.005	0.551		3.483	0.044	0.066
Temporal							
Entorhinal	1.300	0.017	0.258		0.941	0.013	0.335
Fusiform	0.491	0.006	0.486		0.002	0.000	0.965
Inferior Temporal	0.134	0.002	0.715		2.417	0.031	0.124
Middle Temporal	1.742	0.023	0.191		3.671	0.047	0.059
Parahippocampal	1.516	0.020	0.222		0.583	0.008	0.448
Temporal Pole	0.801	0.011	0.374		0.215	0.003	0.644
Transverse Temporal	0.053	0.001	0.819		1.641	0.023	0.204
Superior Temporal	0.795	0.010	0.375		0.223	0.003	0.638
Occipital							
Lateral Occipital	0.171	0.002	0.680		0.788	0.010	0.378
Pericalcarine	0.124	0.002	0.725		0.234	0.003	0.630
Precuneus	0.818	0.011	0.369		1.456	0.019	0.231
Subcortical							
Amygdala	0.007	0.000	0.933		0.211	0.003	0.647
Hippocampus	0.319	0.004	0.574		0.048	0.001	0.828

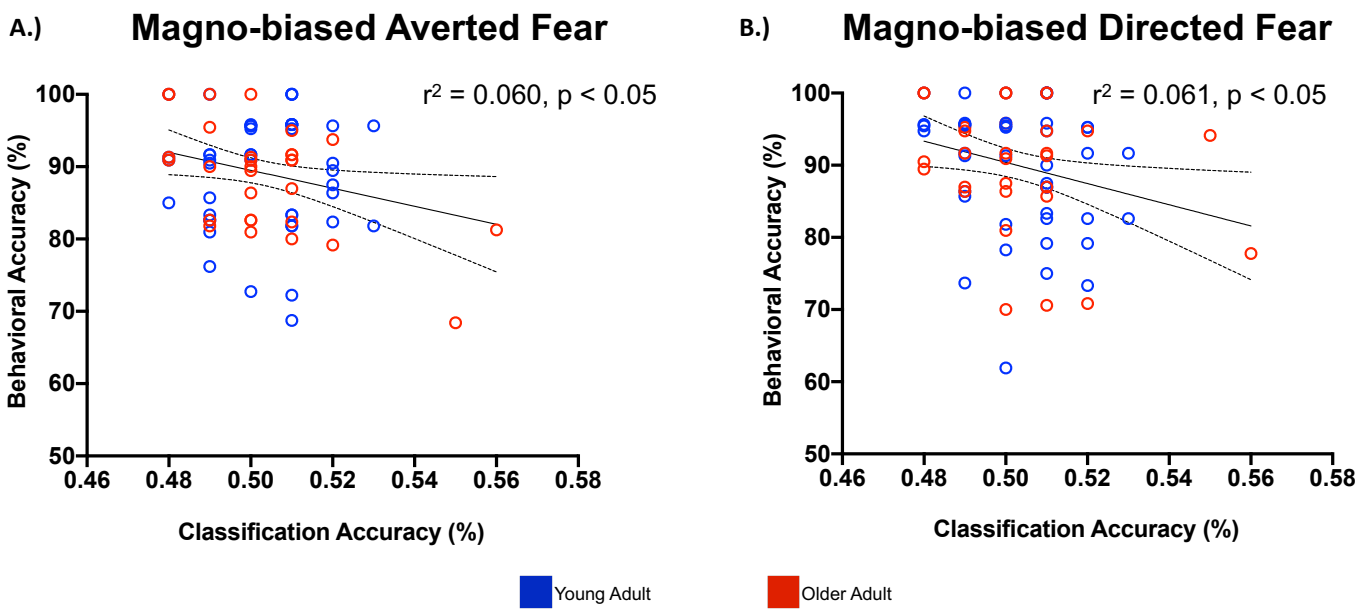

Figure 12. Regression with Classification Accuracy for Magno-biased/Parvo-biased Stimuli and Behavioral Accuracy for Magno-biased Threat Stimuli

Chapter 4

Discussion

The first goal of the current study was to investigate whether regions throughout the ventral visual pathways differentially responded to faces with respect to whether the stimuli were biased towards the magnocellular or parvocellular pathways. A second main goal of the research was to determine if there was age-related dedifferentiation within the magnocellular and/or parvocellular visual pathways in processing the biased face stimuli. A third and final main goal of this study was to explore how age-related dedifferentiation within the magnocellular and/or parvocellular visual pathway influenced threat detection. Specifically, I sought to test if neural patterns of activation to magno- and parvo-biased faces could be discriminated using an MVPA classifier trained on biased face stimuli. For this, I used a previously published dataset designed to test magnocellular and parvocellular biases with respect to the emotion of a face (Im et al., 2017). I employed a multivariate approach to characterize the pattern of neural activity during an emotional discrimination task using the magno- and parvo-biased face stimuli. I then characterized specificity of neural activity by extracting beta weight activation for magno- and parvo-biased face stimuli. Finally, I measured effects of aging by computing multiple regressions with classification accuracy for each ROI and age, separately. My findings revealed that neural patterns of activation for these two conditions can be differentiated within regions comprising both the magnocellular and parvocellular pathways. Specifically, I saw an effect of neural discriminability within left pars opercularis, right pars triangularis, right superior frontal gyrus, left fusiform gyrus and right hippocampus. However, I only saw scant evidence of dedifferentiation in the left pars orbitalis and left inferior temporal gyrus, as shown by decreasing classification accuracy as age increased across our sample, which was not significant. In addition, patterns for magnocellular and parvocellular stimuli were found to be classified reliably from

unbiased face stimuli in regions along both pathways within the left, but not right, hemisphere. Specifically, the left parahippocampal gyrus classified stimuli above chance for magno/unbiased faces, while for the parvo/unbiased classification both the left medial orbitofrontal cortex and left transverse temporal showed similar effects.

Finally, I saw multiple effects when using and MVPA classifier to classify neural patterns of activation associated with facial expression, as well as how behavioral detecting threat relates to distinctiveness of neural patterns. Neural patterns of facial expression for magno-biased stimuli were found to be classified reliably in the left entorhinal gyrus, right amygdala, and right frontal pole. Additionally, neural patterns of facial expression for parvo-biased stimuli were found to be classified reliably in the left hippocampus and right cuneus. When considering behavioral responses, main effects were found for face expression and eye gaze, with neutral faces being more accurately identified as well as when faces had a direct gaze. In addition, the left pars orbitalis, right amygdala, and right hippocampus all have negative relationships with the accurate detection of facial threat. Each finding is discussed at length below.

Neural Representation within Magnocellular and Parvocellular Pathways

The core results revealed clusters along both the magnocellular and parvocellular pathways which successfully classified neural patterns associated with magno- and parvo-biased stimuli. These regions included the left pars opercularis, right pars triangularis, and right superior frontal gyrus which are included within the magnocellular pathway, as well the left fusiform gyrus and right hippocampus which are included within the parvocellular pathway (Kveraga et al., 2007a). Interestingly, these regions are considered to form the endpoints of each of pathways, respectively, with the only exception being the fusiform (Ungerleider & Mishkin, 1982; Kveraga et al., 2007b). While both pathways travel through the LGN and into the occipital lobe, their trajectory through the brain diverges from here. The magnocellular pathway runs dorsally, extending through higher order areas of occipital cortex, through the parietal lobe and eventually terminating in frontal cortex (Kveraga et al., 2007a), where a majority of the significant clusters

were found. The parvocellular pathway runs ventrally from the occipital cortex, though the temporal lobe with termination points in anterior temporal pole and subcortical areas (Kveraga et al., 2007a). With this, the results show that the neural representation for visually biased stimuli is indistinguishable in early visual regions and early in the division of the magnocellular and parvocellular pathways. It isn't until the pathways split and reach their final destination for processing, that being the terminal endpoints of each visual pathway, that neural patterns are distinguishable. Thus, the results conclude that neural specialization within each pathway is more distinguishable in anterior as opposed to posterior portions of each pathway. In other words, these pathways represent direct lines of communication for visual information, in that information enters a pathway and follows the entirety of the path to a processing endpoint, with neural activity becoming more discriminable in those anterior endpoints.

This finding supports work regarding the magnocellular pathway and its function. For example, multiple studies suggest that visual-object recognition is aided by magnocellular projections to the frontal lobe (Bar et al., 2001; Bar, 2003; Bar et al., 2006; Carrietié et al., 2006; Kveraga et al., 2007b). It is posited that the magnocellular pathway sends low spatial frequency information to the orbitofrontal cortex in an effort to identify "candidate objects" which match the image, which in turn are sent to the temporal lobe to aid in object identification (Bar et al., 2001; Bar, 2003; Bar et al., 2006; Kveraga et al., 2007b). This would suggest although these pathways run throughout the brain, only regions involved in the processing of this stimuli show effects of activation of differentiation of neural patterns across magno- and parvo-biased stimuli. This is reflected in the current findings of successful classification in the pars opercularis and triangularis, which overlap with sections of orbitofrontal cortex, and the fusiform gyrus which encompasses much of the temporal lobe. The current regions exhibiting successful classification of magno- and parvo-biased stimuli map onto the proposed low spatial frequency facilitation model for the magnocellular pathway (Bar, 2003; Bar et al., 2006; Kveraga et al., 2007b). Additionally, because the magnocellular pathway runs dorsally through regions that are not

involved with processing of visual stimuli directly, it is possible that none of these regions were differentially activated by the biased stimuli, resulting in the no classification differences along this pathway. In other words, if the regions are not organized in such a way as to process visual stimuli, then it would not process either condition differently. For example, areas of motor cortex located along the dorsal stream will not aid in processing of static image stimuli. However, areas of frontal cortex do process visually imagery and are actually part of the face processing system (Haxby et al., 2001; Gobbini & Haxby, 2007; Elbich et al., 2019). Additionally, areas of frontal cortex have been implicated in processing of visually biased objects and faces (Bar et al., 2006; Kveraga et al., 2007a; Im et al., 2017). Overall, the current results of successful discrimination in anterior frontal regions could be reflective of this top-down predictive process engaged in by orbitofrontal cortex.

In contrast, the parvocellular pathway resides primarily in the temporal lobe, which is populated almost entirely with visual processing regions (Haxby et al., 2000; Gobbini & Haxby, 2007; Kveraga et al., 2007a; Duchaine & Yovel, 2015). Therefore, parvocellular stimuli are more likely to activate regions near or along the pathway, as revealed in the significant clusters for the left fusiform and right hippocampus. Given that the fusiform is highly selective to face stimuli, its appearance here could be reflective of the perception of the parvo-biased facial stimuli, either engaging in processing face recognition (Huang et al., 2014; Elbich & Scherf, 2017) or face expression (Ganel et al., 2005; Harry et al., 2013). With respect to the hippocampus, given that the faces within each condition were identical, it is therefore possible that identities became familiar over the course of the experiment. The hippocampus is situated spatially close to face regions responsible for encoding face identity (Haxby et al., 2000; Kriegeskorte et al., 2007; Duchaine & Yovel, 2015). Thus, it is possible the hippocampus was engaging in retrieval for some facial identities. A way to test these hypotheses would be to have each subject perform a face recognition task after the scanner task. Using these faces and comparable lures, having subjects engage in a task where they explicitly report if they have seen these faces before would

test if the face had been encoded and remembered from the scanner task. This would support that the face processing system is encoding these faces and they are being stored. In sum, the results of parvo-biased map onto previous work with facial identity and familiarity in the ventral temporal lobe, suggesting recruitment of these regions for judgement/perception of face expression.

An important caveat to these findings of significantly above chance classification between magno-biased and parvo-biased stimuli is that early visual regions did not show any above chance classification. However, this is not a surprising result for numerous reasons. First, both these pathways share a common starting point, beginning at different layers of the lateral geniculate nucleus and then projecting to different but adjacent layers in primary visual cortex (V1) (Perry et al., 1985; Callaway, 2005; Kveraga et al., 2007a). Because of they are spatially close, cellular activation differences at the voxel level would be hard to detect with the proposed analyses. Analogous to the "crossing-fibers" problem in diffusion imaging, a single voxel is likely to contain thousands of neurons, potentially populated by both magnocellular and parvocellular cells. This balance would essentially wash out any stimulus specific effects, as a voxel would exhibit roughly equated activation patterns to both types of biased-stimuli. Second, while V1 is responsible for processing basic visual information, higher order visual regions, regions further along the visual processing stream running dorsal, are responsible for processing visual aspects of stimuli that do not exist in the present stimuli (Zeki, 1978; Orban et al., 2004; Senior et al., 2010). Specifically, while primary visual cortex acts as a general funnel for the majority of visual information entering the brain (Tootell et al., 1998), higher order vision areas (V2/3/4a/5/MT) involve processing of spatial orientation, color, and motion orientation of stimuli (Zeki, 1978; Orban et al., 2004; Senior et al., 2010), and are areas within which the magnocellular stream predominantly resides (Ungerleider & Mishkin, 1982; Mishkin et al., 1983; Goodale & Milner, 1992). So, in terms of visual similarity, the stimuli are identical in all visual attributes with the exception of color, which was the experimental manipulation to bias the visual pathways.

In addition, due to the experimental control, the same set of images (e.g., faces) was presented for all conditions, the magno- and parvo biasing being the only difference. Therefore, it is likely that the large number of similarities between the two conditions made it difficult for the classifier to distinguish between conditions in the early visual regions. In addition, because the fusiform is a downstream visual processing region selective to face stimuli, the finding of distinguishable neural patterns here is in line with the function of the region.

Finally, the task in the scanner could play a role in which regions were recruited for detecting the difference. Recall, the task participants engaged in was discriminating emotional expression and reporting in a 2AFC test whether the presented stimuli was either neutral or fearful. Completing this task and coming to the correct emotional identification requires both higher order decision making and processing of the expressive face information – two cognitive processes not centered in posterior visual regions. Decision making generally recruits anterior frontal regions (Fellows & Farah, 2005; Fellows, 2006; Collins & Koechlin, 2012), while face and emotion processing recruit ventral temporal and subcortical regions (Gur et al., 2002; Habel et al., 2007; Gobbini & Haxby, 2007). Despite the fact that neutral and fearful expressions were presented within the context of biased stimuli characteristics (i.e., magno/parvo/unbiased fear, magno/parvo/unbiased neutral), the relative complex judgement may have made the bottom-up recruitment of more primary visual regions moot as they were not necessary to complete the task (See *Differential Neural Patterns to Facial Expression for Magno- and Parvo-Biased Stimuli* for more detail).

In order to determine whether successful classification could be associated with greater response to biased category response (e.g., greater magno-biased beta weight activation in a magno region or greater parvo-biased beta weight activation in a parvo region), each cluster was used as a seed to extract beta weights for magno- and parvo-biased conditions separately. These weights were used for a direct comparison between the overall level of activation to magno- and parvo-biased stimuli within each region. Despite differences in the pattern of neural activity

detectable with the MVPA classifier, the overall BOLD signal within each ROI did not significantly differ (Table 4; Figure 4a-d). One possible explanation for this is that while the visual pathways are mostly dissociated and predominantly one cell type, there still are some cells of different types found along the pathways (Kveraga et al., 2007a; Adams et al., 2019). In other words, there are some parvocellular cells found along the magnocellular path, and vice versa. It is then possible that with the spatial broad measurement of fMRI that voxels contained both cell types instead of one, resulting in a more equitable activation for both conditions rather than biasing towards one stimulus/cell type.

Despite significant differences in the univariate analysis, the observed pattern of response for beta weight activation within these regions show the expected pattern of BOLD differences. Specifically, magno-biased activation is greater than parvo-biased activation in the magno regions of left pars opercularis, right pars triangularis, and right superior frontal gyrus, while parvo-biased activation is greater than magno-biased activation in the right hippocampus (Figure 4a-d). This suggests that, while not statistically significant, regions through with the magnocellular pathway travels show greater activation to magno-biased over parvo-biased stimuli. In addition, the region through with the parvocellular pathway travels show greater activation to parvo-biased over magno-biased stimuli. The non-significance of the results is contrary to what would have been predicted given the findings on magno- and parvo-biased responses in the brain. This could potentially be the result of stimuli suppression for the conditions. Given that there are only 24 novel identities overall, each condition contains four replicants of the same identity with different gaze pattern and emotional expression (Im et al., 2017). Collapsing across these non-independent trials might not afford enough power to detect the hypothesized stark differences. Similar to this, the effects might also be blunted due to the same faces being used across both conditions. Therefore, it is possible that the blunted beta response for each condition within these regions could be the result of either effects of stimulus similarities both within and across condition or the potential presence of both magnocellular and parvocellular cells within voxels, or both.

In sum, using a MVPA classifier, neural patterns of activation for magnocellular and parvocellular are able to be differentiated in multiple regions in both pathways, specifically frontal and temporal/subcortical regions. However, none of these regions showed selectivity to either biased condition when tested with univariate analyses. This suggests there is something unique about the neural patterns for magnocellular and parvocellular information within these regions which cannot be explained by univariate differences.

Dedifferentiation within Magnocellular and Parvocellular Pathways

The second goal of the study sought to investigate whether the magnocellular and parvocellular pathways exhibit age-related dedifferentiation in their response to biased stimuli. Dedifferentiation is a well-known effect in the aging literature, with multiple studies showing that older adults exhibit decreases in the neural specialization of specific classes of stimuli or cognitive operations (Park et al., 2001, 2004, 2012; Park & Reuter-Lorenz, 2009; Carp et al., 2011a,b; Dennis & Cabeza, 2011; Papenberg et al., 2011). This is especially true of later stage visual regions populating the ventral temporal lobe (Park et al., 2004, 2012; Carp et al., 2011b). For example, Park & colleagues (2004) showed participants images from 5 distinct categories: faces, houses, chairs, pseudowords and phase scrambled images. The participants were asked to remember each image and while fMRI activity was recorded across regions in visual cortex, with a focus on regions known to support processing of each stimulus type. The results showed an interaction with age, wherein younger adults exhibited greater category-specificity compared to older adults (i.e., greater activation to faces than houses in the fusiform for younger adults, with a lower magnitude difference for older adults). This shows that specialization is reducing in healthy aging, with brain regions being recruited more often to aid in processing.

Given the fact that dedifferentiation is seen across visual categories of stimuli, I sought to investigate whether age-related dedifferentiation of physical properties of stimuli, such as contrast and color, critical to the engagement of magnocellular and parvocellular neurons, would also exhibit reduced responsivity in aging. This hypothesis was tested by taking the classification

accuracy distinguishing magno-biased and parvo-biased stimuli from each individual ROI for all subjects and entering them into separate regressions predicting age. Overall, the results showed no effect of dedifferentiation within either pathway when correcting for multiple comparisons. However, the results identified two regions that exhibited a negative relationship between neural selectivity and age, specifically the left pars orbitalis and left inferior temporal gyrus (Figure 5). The negative relationship indicates that as age increases, the neural patterns underlying magnocellular and parvocellular images are less distinct. While the foregoing analysis offers limited evidence for age-related dedifferentiation with regard to magnocellular and parvocellular stimuli, it may be important to note that 50 regions identified along the magnocellular and parvocellular pathways did not show any evidence of age-related dedifferentiation. This would suggest that the process of dedifferentiation does not occur within the magnocellular and parvocellular pathways.

However, it must be noted that there are some important distinctions between the question addressed here and evidence of age-related dedifferentiation in the rest of the literature. Much of the prior work on dedifferentiation has been done with gross categorical differences between stimuli conditions. For example, the study from Park and colleagues (2004) mentioned above defined their neural specialization by looking within regions associated with the processing of each stimulus type and compared activation to “within” and “between” activation (e.g., comparing all t-values from the fusiform, a face processing region) (Park et al., 2004; Kanwisher et al.,1997). In a later study, Park and colleagues (2012) employed a similar approach, this time just using faces and houses. The resultant dedifferentiation findings were the same – regions specializing in the processing of a face showed greater activation to houses for older adults compared to younger (Park et al., 2012). Using multivariate methodology, Carp and colleagues (2011b) sought to quantify dedifferentiation by employing multivariate pattern analysis to compare the same conditions in Park et al., 2004, specifically faces, pseudo-words, houses, and chairs. However, their metric of similarity was different. They employed a neural distinctiveness

metric, comparing the correlation values between all within-condition trials to the correlation of all between condition trials (Carp et al., 2011b). Conceptually though the comparison is the same, whereby activation/correlation of the same conditions should be greater than between conditions. The results were convergent with the prior findings: older adults exhibited decreased specialization for conditions within regions specialized for that region (i.e., increased activation for non-house images in the parahippocampal gyrus, an area of house/place processing) (Carp et al., 2011b). In other words, between-condition correlations were more similar to within-condition correlations in older adults but not younger (Carp et al., 2011b).

In each of these studies, dedifferentiation was established by comparing activation within a known region of selectivity for a specific stimulus type for that exact stimulus and one that should elicit lower activation. However, the comparison here was not across visual category but different physical properties within the same category of stimuli, namely faces. In effect, this study goes one step beyond previous work by examining dedifferentiation of visual image properties rather than gross categorical differences. With the overall null findings of dedifferentiation, this would suggest that declines in neural specificity in aging are not ubiquitous in the brain, and that it can be dependent on type of neuron as well as function (i.e., detect visual information or process visual information).

Secondly, it should be noted that there is an experimental confound that may have influenced these overall findings, specifically individualized well-controlled stimuli biasing. That is, it is possible that the rigorous process by which the biased stimuli were created dampened or negated potential dedifferentiation results. Generally speaking, visual stimuli in the world do not adapt to meet deterioration of the visual system across age. While some of these defects can be corrected for (e.g., glasses, contacts), visual properties do not dynamically alter to provide us the best and most precise visual clarity. It has also been shown that older adults do show deficits in detecting biased stimuli, especially when biasing the magnocellular pathway, beginning around age 50 (Benedek et al., 2017). However, in the case of the present dataset, one of the important

controls was to ensure that all subjects could not only see the stimuli but also match the level of biasing to individual subject thresholds, a process that is not done in everyday life. In addition, the previous work on dedifferentiation also shows no effort to alter stimuli to be more or less detectable for each individual, let alone between age groups (Park et al., 2004; Dennis & Cabeza, 2011; Carp et al., 2011b; Park et al., 2012; Bowman et al., 2019). It is possible that the enhanced contrast in the biased stimuli for older adults counteracted or accounted for potential deficits or differences in processing. However, because stimuli were adjusted to each subject's own visual acuity in the current study, biased stimuli created for the older adults could have accounted for this discrepancy, creating a stimulus set that was more easily detectable in the face of these age-related changes. In other words, the process for individualizing stimuli to each viewer could have corrected potential problems with detecting similar visual stimuli the person would see in the general environment. This could mean that aging effects on visual acuity could be a confounding factor for the previous work on dedifferentiation in the visual system. While many studies correct for visual impairments, very few correct for individual sensitivities to contrast and luminance.

Finally, there is the possibility that the classic way we currently think about dedifferentiation is not actually possible for these visual pathways. Much of the work shows that dedifferentiation occurs within brain areas as they exhibit increased activation for other stimuli types for which they are specialized. This is a common approach/finding both in the visual domains (see above) as well as in other cognitive domains. In memory, for example, dedifferentiation in learning has been shown as activation differences with respect to types of learning (Dennis & Cabeza, 2011). Here, older adults showed roughly equated activation to different learning strategies in the caudate, putamen, and bilateral medial temporal lobe, while young adults show greater activation to explicit learning in the medial temporal lobe and implicit learning in the caudate & putamen (Dennis & Cabeza, 2011), This process of becoming less selective via increased activation to a new/different stimulus may not be the case of these visual pathways. Due to their cellular architecture, each cell cannot become sensitive to other types of

information. In other words, a magnocellular cell cannot become sensitive to color information, and a parvocellular cell cannot become sensitive to low spatial frequency information. Each is so specialized that there is no room for becoming sensitive to other forms of visual information. They can become less sensitive over time, especially the magnocellular pathway showing decreases in sensitivity beginning around 50 (Benedek et al., 2017). However, this decrease will never be accompanied by an increase in sensitivity to parvo-biased information. One way to test this hypothesis would be to use a method similar to Denison and colleagues (2014). In this study, the researchers used a functional localizer task with gabor patches biased for either magnocellular (i.e., grayscale, low contrast) or parvocellular (i.e., green & red, high contrast) cells to identify clusters of activation (e.g., ROIs) for one condition over the other (Denison et al., 2014). If functional regions could be identified which were selective to either magnocellular or parvocellular information, these could serve as test regions for longitudinal examination. Over time, these functional patches should become less sensitive to their respective specialization type, while the non-specialized visual condition should exhibit no change.

In sum, regions along the magnocellular and parvocellular pathways do not exhibit age-related dedifferentiation for their biased stimuli. Given the current way we measure and conceptualize this process, it may not even be possible for these pathways to become dedifferentiated. Specifically, there seems to be a distinction between specialization defined functionally compared to biologically. The cells which comprise both pathways may have the capacity to become less sensitive (i.e., reduced activation/amplitude) over time (e.g., with age), but they may never become *more* sensitive to, or exhibit any greater activation toward, a stimulus for which they are not selective. This is in contrast to what is observed in “classic” dedifferentiation, where there is always some observed activity to the non-selective category (e.g., neurons in fusiform gyrus fire in response to objects, but typically show greater activation to faces). An ideal, albeit difficult, way to test this would be to identify magnocellular and parvocellular cells in the macaque brain and present them biased stimuli across age range

spanning young and old age, measuring if either or both cells become sensitive to visual properties of the other cell type.

Neural Representation of Unbiased Faces within Magnocellular & Parvocellular Pathways

I also sought to interrogate differences in discriminability along the magnocellular and parvocellular pathway with respect to unbiased face stimuli (i.e., faces that are not magno- or parvo-biased). The unbiased face condition had visual properties which are sensitive to both the magnocellular (i.e., no color, visual contrast) and parvocellular (high-contrast difference), therefore acting as a good control for both visual pathways. The hypothesis here was that neural patterns for both conditions of visually biased stimuli (i.e., magno-biased and parvo-biased) would be distinguishable from unbiased stimuli along the same pathways noted above. In addition, activation in regions that showed above chance classification would be greater for the visually biased condition compared to the unbiased condition. This hypothesis was tested by training two new MVPA classifiers. The first classifier was used to test magnocellular selectivity and was trained with only magno-biased and unbiased images, Conversely, the second classifier was used to test parvocellular selectivity and was trained with only parvo-biased and unbiased images.

The results of the magno-biased/unbiased classification showed multiple clusters of successful classification within both pathways, including the left parahippocampal gyrus and left transverse temporal gyrus. Additionally, the parvo-biased/unbiased classification showed significant clusters in the left medial orbitofrontal. Overall this shows that visually biased and unbiased images can be successfully distinguished at points along both magno and parvo cellular pathways. While neither of these regions overlaps with the prior findings for classifying magno-/parvo-biased stimuli (see Results: Dedifferentiation of Magnocellular and Parvocellular Pathway), they do map on to specialized regions for each pathway. First, in the magno/unbiased classification analysis, the result of the left parahippocampal and left transverse temporal gyri fits with the exclusive visual properties of mango-biased and unbiased stimuli. With regard to the

physical differences between the two stimuli conditions, the difference between magno-biased and unbiased stimuli is the level of contrast in the image, with unbiased images having a higher visual contrast between the face and foreground. It is likely that the commonalities between these visual conditions were indistinguishable (i.e., both lack color), but the differences were able to be detected by the classifier. This can be seen in the results where regions which would be selective to the visual commonalities (i.e., magno-biased regions) did not significantly classify neural differences between the two conditions. However, regions which were selective to the unique properties (i.e., high visual contrast) were able to successfully distinguish between the two conditions, which in this case were the parahippocampal and transverse temporal gyri. In essence, the magnocellular properties of each image cancelled each other out and only the parvocellular properties remained to distinguish the neural patterns. The inverse argument can be made for the parvo/unbiased classifier. Here, the key difference between the parvo-biased and unbiased stimuli is that the parvo-biased is red-green colored while the unbiased is black and white. Again, the commonalities between these visual conditions were likely indistinguishable (i.e., high visual contrast), but the differences were able to be detected by the classifier. The results show that regions selective to the commonalities (i.e., parvo-biased regions) were not above chance, but mango-biased regions like the medial orbitofrontal cortex were. Essentially, the results from each classification analysis produced results in the opposite pathway, suggesting that the commonalities with the unbiased stimuli were equitable at the level of representation which resulted in the selection of non-common features. This would explain why a magno/unbiased classifier showed significant classification in a parvo-related region, and why a parvo/unbiased classifier showed significant classification in a magno-related region.

In order to determine whether successful classification could be associated with greater response to biased category response (e.g., greater parvo-biased beta weight activation in a parvocellular region versus unbiased activation), each cluster was used as a seed to extract beta weights for parvo-biased and unbiased conditions separately. These weights were used for a

direct comparison between the overall level of activation to parvo-biased and unbiased stimuli within each region. This result showed that overall BOLD signal within the left transverse temporal gyrus was greater for unbiased stimuli compared to parvo-biased stimuli (Figure 6). A possible explanation for this is the differential effect of color-biasing high-contrast images and simply high-contrast images. One study sought to test the effects of isoluminant chromatic (red-green/parvo-biased) and achromatic (black-white/unbiased) sinusoidal gratings in the parvocellular system while measuring VEPs using EEG (Tobimatsu et al., 1996). Each grating was a high-contrast image as to bias only towards parvocellular cells (Tobimatsu et al., 1996). Their results showed different peaks of activation based on the degrees of contrast. The peak amplitude for the isoluminant chromatic condition was found in lower contrast, most likely the result of the color-sensitive aspects of the parvocellular system (Tobimatsu et al., 1996). In contrast, the peak amplitude for achromatic condition was found in gratings which had a higher contrast than those of the isoluminant chromatic condition, supporting their increased sensitivity to high-contrast images (Tobimatsu et al., 1996). Overall this suggests that while the parvocellular system is sensitive to both of these visual properties, the actual pattern of activation is not identical. Therefore, the results show that the patterns of representation for two forms of parvocellular information are not the same and actually map onto different sensitivities within the same system.

In terms of gauging effects of aging, I sought to investigate whether age-related dedifferentiation for physical properties of biased stimuli compared to unbiased stimuli would also exhibit reduced responsivity in aging. This hypothesis was tested by taking the classification accuracy distinguishing magno-/unbiased and parvo-/unbiased stimuli from each individual ROI for all subjects and entering them into separate regressions predicting age. Overall, the results showed no effect of dedifferentiation within either pathway when correcting for multiple comparisons. However, the results identified multiple regions showing either positive or negative relationships between neural selectivity and age. For the magno-biased comparison, the right

parahippocampal gyrus showed a positive relationship with age (Figure 7a). However, for the parvo-biased comparison, there are multiple mixed effects. The left amygdala exhibits a negative relationship with age, while the left caudal anterior cingulate, left parahippocampal gyrus, and right precuneus all show positive relationships with age (Figure 7b-e). The mixed findings show that within the left amygdala, as age increases, the neural patterns underlying magnocellular and unbiased images are less distinct. However, four other regions along both pathways show that as age increases, the neural patterns for unbiased compared to magnocellular/parvocellular images are more distinct. Interestingly, this includes regions along both magnocellular and parvocellular pathways. One potential explanation for this is the reduced response to magno-biased stimuli in older adults. Recent EEG work has shown that older adults do show deficits in detecting magnocellular and parvocellular biased stimuli, with effects being greater for magno-biased stimuli (Benedek et al., 2017). This deficit begins around age 50 and is noted as an increase in latency and decrease in amplitude (Benedek et al., 2017). Given that unbiased stimuli have properties of both, it is possible that while biased stimuli show decreased amplitude, the unbiased stimuli do not follow a similar pattern. Because both pathways are sensitive to unbiased stimuli, both magnocellular and parvocellular cells in a given voxel could be activated by it, whereas the visual biased conditions can only activate one cell type. This difference in activation level could influence the neural pattern to the point where the classifier could detect it. While the foregoing analysis offers very limited evidence for age-related dedifferentiation with regard to biased/unbiased stimuli, it is important to note that 47 regions identified along the magnocellular and parvocellular pathways did not show any evidence of age-related dedifferentiation, with some showing the complete opposite effect. Together with the above findings from the magno/parvo dedifferentiation analysis, this evidence suggests that the process of dedifferentiation does not occur within the magnocellular and parvocellular pathways.

Differential Neural Patterns to Facial Expression for Magno- and Parvo-Biased Stimuli

Finally, to answer the question of whether successful classification of facial expression could be achieved within the magnocellular and parvocellular pathways, a MVPA searchlight analysis was conducted within the magno- and parvo-biased conditions separately. For this, the MVPA classifier was trained to distinguish between fearful and neutral faces for a single biased stimulus set (i.e., a classifier analysis run on magno-biased stimuli and a second on parvo-biased stimuli). The results of these two analyses show multiple clusters of successful classification within both pathways, including the left entorhinal gyrus, right amygdala and right frontal pole for magno-biased stimuli, and the left hippocampus and right cuneus for parvo-biased stimuli. In order to test for selectivity for facial expression, beta weight activation was extracted for fearful and neutral faces separately. There were no differences in activation between fearful and neutral faces within either region (Figure 8). However, there was a trend in the right amygdala with fearful faces showing overall greater activity than neutral faces, which is expected based on previous face emotion research (Adolphs et al., 1995; Pillay et al., 2006; Sato et al., 2004; McFayden et al., 2019).

These regions, in part, overlap with previous work studying both visual pathways and face processing. For example, the face processing system is comprised of multiple regions throughout the brain, but is primarily located in the ventral occipital temporal cortex (Bruce & Young, 1986; Haxby et al., 2000; Gobbini & Haxby, 2007). The core areas of this system reside mostly in the middle and posterior temporal lobe, while extended regions include the anterior temporal lobe, ventromedial prefrontal cortex, and the amygdala (Haxby et al., 2000; Gobbini & Haxby, 2007). These extended areas process information related to emotional expression, mental states, and familiarity (Gobbini & Haxby, 2007). The magno-biased clusters overlap almost entirely with extended network face-processing regions, the only exception being entorhinal cortex. However, there is some evidence that fearful faces are better remembered than positive or neutral faces, even if the exposure is implicit (Milders et al., 2011; Yang et al., 2011; Wang, 2013). Given the proximity of entorhinal cortex to the hippocampus and other areas of the face

processing network implicated in emotional and familiarity processing (i.e., the amygdala and anterior temporal pole), it is possible the entorhinal cortex is playing some role in the processing of these faces as well.

In addition, these findings also fit with previous work conducted with this dataset. Specifically, Im and colleagues (2017) found that the right amygdala showed increased activation for clear threat (i.e., averted gaze and a fearful emotion) compared to ambiguous threat (i.e., direct gaze and fearful emotion) for magno-biased stimuli (Figure 9). However, the converse finding of ambiguous threat being greater than clear threat in the left amygdala for parvo-biased images was not found here. While the exact comparison was not done for the univariate and multivariate analyses, it does provide convergence that the right amygdala is showing similar effects for processing facial threat cues.

Interestingly, disruptions in magnocellular pathway have also been found in clinical samples which have deficits in emotion processing. Those with schizophrenia have been shown to have disruptions in both of these pathways (Hooker et al., 2002; Kosaka et al., 2002; Martínez et al., 2008; Butler et al., 2009; Norton et al., 2009; Bedwell et al., 2013; Chieffi, 2019). For example, Norton and colleagues (2009) had schizophrenic patients and controls engage in a contrast detection task and an emotion discrimination task. For the contrast detection, subjects were shown sinusoidal gratings of varying contrast levels and where asked to judge if the first or second was a target (Norton et al., 2009). The emotion discrimination measured the just noticeable difference between the emotion face and neutral using morphed emotion faces of: 6, 12, 24, 48 and 100% intensity (Norton et al., 2009). They found that those with schizophrenia needed a greater threshold of intensity to correctly identify the emotion at the rate of 80% compared to controls (Norton et al., 2009). In addition, accuracy on the contrast detection task was positively correlated with performance in the emotion discrimination for those with schizophrenia, such that those with more difficulty discriminating basic contrasts had worse performance discrimination emotional expression (Norton et al., 2009). This deficit was attributed

to potential issues with function of the magnocellular pathway, which was followed-up on in a study from Bedwell and colleagues (2013). Here, researchers used both showing schizophrenic and control participants and showed them different emotional faces, biasing either the magnocellular or parvocellular pathway (Bedwell et al., 2013). In this task, subjects had to choose from one of four possible emotional labels for the face: happy, sad, fearful, and angry (Bedwell et al., 2013). Overall, schizophrenic participants showed more errors when trying to label sad face expressions with the gray background, but critically also deficits in correctly identifying fearful faces from angry with the gray background as well (Bedwell et al., 2013).

Disruptions in this pathway has also been recorded in those diagnosed with autism spectrum disorder and autism phenotypes (McCleery et al., 2007; Brown & Crewther, 2017; Burt et al., 2017). Autism spectrum disorder is a developmental disorder characterized deficits in social and emotional communication, and is also marked by deficits in the processing of faces (Adolphs et al., 2001; McCleery et al., 2007; Burt et al., 2017). In a sample of high-risk infants, McCleery and colleagues (2007) showed them different visual gratings of light/dark or red/green at different contrast levels, with responses gathered using a forced-choice preferential looking paradigm. Their results show that high-risk infants had a much greater contrast sensitivity to magno-biased gratings, while sensitivity to parvo-biased gratings matched that of controls (McCleery et al., 2007). In other words, high-risk infants needed higher contrast gratings to attend to them, otherwise they would blend into the background and be difficult to see (McCleery et al., 2007). Expanding on this finding of magnocellular deficits, Burt and colleagues (2017) sought to determine if processing of fearful faces is altered by the presence of increased autistic phenotypes. A set of adults with low and high autism phenotypes were shown sets of hybrid faces containing low or high spatial frequency information from fearful or neutral faces, creating 4 hybrid types in total (Burt et al., 2017). They were asked to identify the emotion being displayed on the face while ERPs were collected (Burt et al., 2017). The results showed that while the low phenotype group showed modulation in the P100 where it increased in amplitude for fearful low

spatial frequency hybrids compared to neutral low spatial frequency hybrids (Burt et al., 2017). However, the high phenotype group showed an overall reduction in the P100 and N170 with no effect of emotion of the face or spatial frequency (Burt et al., 2017). Their results suggest that the low spatial frequency information from the fearful face is facilitating recognition of that emotion in those with low autistic traits, but there is no commensurate response in those with high autistic traits (Burt et al., 2017). Overall, this suggests clinical disorders marked by deficits in face processing also exhibit deficits in magnocellular and parvocellular processing. Subsequently, there could be a link between the issues in the two systems, likely the visual pathway subserving function of face processing regions. The potential link via disfunction implies that, in a healthy population, regions involved in face and emotion processing would be activated when presenting this visually biased face stimuli, such as in the present work and findings of the entorhinal gyrus and amygdala.

Interestingly, the findings of the parvo-biased stimuli do not fit with the expected predictions or with previous work, given that the parvocellular pathway travels ventrally. While the hippocampus is a ventral region and adjacent to the parvocellular projections, the cuneus on the other hand is a dorsal visual region. One explanation for this discrepancy can be seen in the peak coordinates for this cluster (Table 9). The peak for this particular cluster is spatially very close to the posterior part of the superior temporal sulcus, a face selective region implicated in processing of changeable aspects of faces, such as expression (Haxby et al., 2000; Gobbini & Haxby, 2007; Duchaine & Yovel, 2015). Additionally, the current models of face processing suggest increased bidirectional connectivity between this region and the fusiform gyrus (Duchaine & Yovel, 2015). It is possible that due to the spatial closeness of these two regions that this cluster includes some voxels from the posterior superior temporal sulcus. These clusters could be receiving information from the parvocellular pathway via the fusiform gyrus, which would account for its activity in distinguishing neural patterns of facial expression. One way to measure this would be to employ an effective functional connectivity approach. Functional

connectivity is the coupling between brain regions, based on the principle of Hebbian learning (i.e., regions that fire together, wire together) (Hebb, 1949; Friston et al., 2003). With this tool, it is possible to determine and quantify if one brain region is providing input to another. Using the timeseries data from this scanner task, I can model if the fusiform is sending information to these voxels or not.

In sum, the classification of fearful and neutral faces for magno-biased stimuli yielded significant clusters in multiple regions of the face processing network. In addition, these regions are implicated in aspects of emotion discrimination and could represent the processing of neural patterns of magno-biased faces. Critically, clinical disorders marked by deficits in emotion processing also exhibit signs of magnocellular dysfunction, further strengthening the hypothesis that these clusters are neural patterns of face emotion information.

Effects of Neural Dedifferentiation on Threat Detection

The final primary question centered around exploring if neural dedifferentiation of magnocellular and parvocellular stimuli had an effect being able to detect emotionality of the face, specifically threating faces. To begin this analysis, first I created a mixed model ANOVA to include expression (fear/neutral face), visual pathway (magno/parvo), and gaze (direct/averted) as IVs and behavioral accuracy as the DV, with age as a covariate of interest. Because the goal of the previous work using this data focused on anxiety, age was controlled for, but did not explicitly investigated for its relationship with the data (Im et al., 2017). Therefore, this analysis serves as an initial examination of how age influences behavioral response to threat detection. My results showed two main effects of expression and gaze. Overall, neutral faces are more accurately detected compared to fearful faces, and faces with directed gaze are more accurately identified than faces with averted gaze. There was a trend for significance with respect to visual pathway ($p = 0.07$), with magno-biased trials being more accurate that parvo-biased trials. However, there were no interactions with any IV and age. This suggests that while participants showed increased accuracy based on expression and gaze direction, these differences were not

attributed to age. A potential reason for these differences could be due to the visual-biasing process. The transformation from the original database photos, which are higher resolution and color, to the contrast outline of facial features for all biasing conditions could have made it difficult to detect the differences in facial expression and eye gaze. For example, gauging eye gaze differences can be more difficult when the subtle contrast differences are gone (i.e., pupil, eyelid, eyebrow, and hair are a single color). Similarly, subtle markers for expressions employing lip and eye contours might be lost (i.e., lips, eyelids, defining face line are a single color). One way to test this hypothesis would be to use the original stimuli along with the visually biased stimuli to see if the processing of making judgements with biased stimuli makes the overall task more difficult behaviorally.

I also sought to investigate if dedifferentiation in the magnocellular and/or parvocellular pathways impacts one's ability to detect threat in either or both visual pathways. As discussed previously, dedifferentiation is a common phenomenon found in aging, especially in the ventral temporal lobe (Park et al., 2001, 2004, 2012; Park & Reuter-Lorenz, 2009; Carp et al., 2011a; Dennis & Cabeza, 2011; Papenberg et al., 2011). This hypothesis was tested by entering classification accuracies for magno- and parvo-biased stimuli within each region into a regression with behavioral accuracy for threat detection as the dependent variable. Overall, the results showed no effect of dedifferentiation within either pathway when correcting for multiple comparisons. However, the results showed that for magno-biased clear threat (averted fear faces) there were negative relationships with the right amygdala, right hippocampus, and left pars orbitalis. For magno-biased ambiguous threat (directed fear faces), there is a negative relationship with the right hippocampus. Finally, for the parvo-biased ambiguous threat (directed fear faces), there was a negative relationship with the left pars orbitalis. However, when accounting for multiple comparison correction, these results suggest that the process of dedifferentiation does not occur within the magnocellular and parvocellular pathways.

Despite the non-significance of the findings, some of the results do converge with previous work with this dataset. Referring again to Im and colleagues (2017), the current results of decreasing classification accuracy with age in the right amygdala converge with their main effect of the right amygdala showing increased activation for clear threat compared to ambiguous threat for magno-biased stimuli. In addition, the right hippocampus and left anterior orbitofrontal cortex showed a similar effect in their data, mapping onto the current findings for the same stimulus type (clear threat) within the right hippocampus and left pars orbitalis, which while not the same region is a spatial neighbor (Im et al., 2017).

Interestingly, the findings for magno- and parvo-biased ambiguous threat do not converge with previous work. One possibility for why this might be so for the right hippocampus is that this region might have distinguishable patterns for both clear and ambiguous threat. This would fit with the previous work showing a selectivity to magno-biased clear threat, which could underlie a distinct neural representation for clear threat. In other words, for the right hippocampus to be selective to a specific type of threat, it must have both some representation of what stimulus type it is and what it is not (e.g., a face not a car). Therefore, while univariate findings show the selectivity, the relationship of classifier to accuracy implies there is a pattern for each type of threat. One way to test this would be train the classifier on only magno-biased clear and ambiguous threat images to determine if they can actually be distinguished.

While the exact comparison was not done for the univariate and multivariate analyses, it does provide convergence that the right subcortical and left frontal regions are showing similar effects for processing facial threat cues. While the foregoing analysis offers limited evidence for age-related dedifferentiation with regard to magnocellular and parvocellular stimuli, it may be important to note that 23 regions identified along the magnocellular and parvocellular pathways did not show any evidence of age-related dedifferentiation. This would suggest that the process of dedifferentiation does not occur within the magnocellular and parvocellular pathways.

Future Directions

There are multiple future directions that can be taken to expand on this work. First of which, to better identify sensitive patches along the magnocellular and parvocellular pathway, a functional localizer task similar to the one employed by Dennison & colleagues (2014) could prove useful. This type of task would have the benefit of answering the questions about visual biasing of cortical brain regions at a visual perceptual level without the complex information carried in a face acting as a potential confound. Additionally, any visually biased regions found using the localizer task can act as regions of interest for further interrogation using the threat detection task. This would increase the robustness of any results because the task to identify and interrogate the regions are now independent.

A second direction, or rather expansion, on this work would be to increase the number of trials for each of the conditions, thereby providing the classifier with more data to refine the model of classification. This would also open the possibility of asking more fine-grained questions about the neural patterns associated with threat. For example, an interesting question would be do the neural patterns for clear threat differ from ambiguous threat when the stimuli are biased toward either visual pathway. This would mirror the univariate analyses performed previously on this dataset (Im et al., 2017; Adams et al., 2019). Presently this analysis would be underpowered to accurately train the classifier, but an increased trial number would mitigate that issue.

A third future direction in this domain would be to isolate the differential effects of the biased stimuli for both pathways. As discussed previously, each visual pathway has two sensitivities. Magnocellular cells are sensitive to low contrast images in addition to motion. Parvocellular cells are sensitive to high contrast in images as well as color. It would be an interesting question if neural patterns within each biasing could be distinguished (e.g., differences in neural patterns for motion and low contrast in pars orbitalis). It would also be curious to note how the results change, if at all, when threat information is visually biased toward a pathway in different ways (e.g., biasing parvocellular with only color or only high contrast). The design

could be similar to how stimuli were created here, with the notable change of altering face stimuli into small video clips to display motion in the stimuli.

Finally, an important direction to take is to obtain a better understanding of how these visual pathways alter with age. While the results show that dedifferentiation is not occurring, there is still evidence that there is some reduction in sensitivity that comes with healthy aging. There is a need for further work to understand what is happening to these cells at the neural level. Realistically, this would involve further non-human primate research to isolate specific magno and parvo cells and measure their selectivity over time. This work could then be extrapolated to and merged with current neuroimaging findings in humans.

Conclusion

This project set out to test whether neural patterns for faces biased toward the magnocellular and parvocellular pathway could be distinguished, if these patterns are dedifferentiated as we age, and if they impacted ability to detect facial threat. To do so, I employed a multivariate approach to distinguish and quantify neural patterns within magnocellular and parvocellular pathways. Overall, I found that neural patterns for visually biased stimuli can be observed in both the magnocellular and parvocellular visual pathways, particularly in anterior frontal and ventral temporal areas of the brain. Specifically, the results show that regions involved in either face processing or the task of identifying/choosing facial expression exhibited distinguishable neural patterns for magno-biased and parvo-biased stimuli. This is supported by the lack of findings in non-related regions, such as motor cortices. Additionally, effects were not seen in more posterior primary regions such as V1 likely due to the large population of both cell types, making visual patterns more difficult to distinguish.

As for the second goal of determining if these neural patterns are dedifferentiated as we age, this was accomplished by using age to predict classifier accuracy for each region along both visual pathways. However, the results here conclusively show that there is no neural dedifferentiation in this signal in either pathway. The hypothesis posited here suggests that

classical dedifferentiation as defined as decreased sensitivity to a preferred stimulus while activation to another remains stagnant or increases does not align with these pathways. Critically, the biological design of these cells is such that they can only be sensitive to the visual properties for which they are already sensitive. There can be no increase in or stagnant activation to visual properties for which the cell is insensitive. This would require a fundamental shift in what the cell is and how it operates, which as of yet is an impossible process.

Finally, the final goal of this project was to identify if neural patterns for magno-biased and/or parvo-biased stimuli impacted ability to detect facial threat. To test this, classifier accuracy for each region along both visual pathways was used to predict behavioral accuracy for detecting facial threat. However, the results show that neural patterns within both visual pathways have no effect on behavioral accuracy. It is possible that due to the classifier information includes aspects of neutral faces, as well as clear and ambiguous threat cues. Future work should revisit this idea and identify distinguishable neural patterns for clear and ambiguous threat, which could prove as a more suitable comparison. Overall, research is the first of its kind to merge visual pathway biasing, multivariate pattern classification, dedifferentiation, and social perception.

Appendix

Figure Legends

Figure 1. Diagram of the Magnocellular and Parvocellular visual pathways from Merigan & Maunsell (1993). Both pathways begin in the retina and track through different cortical regions after V2. Abbreviations: AIT, anterior inferotemporal area; CIT, central inferotemporal area; LIP, lateral intraparietal area; Magno, magnocellular layers of the LGN; MST, medial superior temporal area; MT, middle temporal area; Parvo, parvocellular layers of the LGN; PIT, posterior inferotemporal area; VIP, ventral intraparietal area.

Figure 2. Example trial from Magno/Parvo Localizer taken Denison et al., (2014). Magno-biased stimuli (magno) were low spatial frequency, monochrome gratings while parvo-biased (parvo) were high spatial frequency, high color contrast gratings. During the block, some trials would have a decrease in contrast appear on the screen. Subjects were asked to maintain fixation and count the number of luminance or color (for magno and parvo blocks, respectively) targets that appeared within a block.

Figure 3. Example Pretest for Magno/Parvo Stimuli Creation and Experiment Trial from Im et al., 2017. A diagram of the tasks used to quantify and test visually biased stimuli. Example of magno-biased stimuli creation where subjects' reported the emotional expression of the face, with correct answers decreasing the contrast difference between the face and background (a). Example of parvo-biased stimuli creation where subjects' reported the color needed to make the face appear to stock flickering (b). The example task used in the MRI experiment, where subjects' reported the emotional expression of the face and received feedback (c).

Figure 4. Beta Weight Activation from Magno-biased/Parvo-biased Searchlight Clusters. Plotted bar graph of beta weight activation. Each successful searchlight was used as a mask from which to extract activation for magnocellular and parvocellular trials, separately. Despite no significant effects, pattern of magno-/parvo- magnitude aligns with the predictions and location of each regions along the magnocellular or parvocellular pathway.

Figure 5. Regression of Classification Accuracy for Magno-biased/Parvo-biased Stimuli and Age. Classification accuracy for magno-biased and parvo-biased within the left pars orbitalis was predicted by age (a), as well as in the left inferior temporal gyrus (b).

Figure 6. Beta Weight Activation from Unbiased/Parvo-biased Searchlight Clusters. Plotted bar graph of beta weight activation for the left transverse temporal gyrus, which shows activation to unbiased stimuli is greater than parvo-biased stimuli.

Figure 7. Regression of Classification Accuracy for Magno-biased/Parvo-biased/Unbiased Stimuli and Age. When classifying unbiased stimuli against magno-based stimuli, (a) classification accuracy in the right parahippocampal gyrus was predicted by age. When classifying unbiased stimuli against parvo-based stimuli, age predicts classification accuracy in (b) the left amygdala, (c) left caudal anterior cingulate (d) left parahippocampal gyrus, and (e) right precuneus.

Figure 8. Beta Weight Activation from Visually Biased Fearful/Neutral Searchlight Clusters. Plotted bar graph of beta weight activation for the classification of fearful/neutral stimuli. Each successful searchlight was used as a mask from which to extract activation for magnocellular and parvocellular trials, separately. Despite no significant effects, pattern of

magno-/parvo- magnitude aligns with the predictions and location of each regions along the magnocellular or parvocellular pathway.

Figure 9. Regression of Classification Accuracy for Visually Biased Fearful/Neutral Stimuli and Age. Classification accuracy for magno-biased and parvo-biased within the left amygdala was predicted by age.

Figure 10. Regression with Classification Accuracy for Magno-biased/Parvo-biased Stimuli and Behavioral Accuracy for Magno-biased/Parvo-biased Threat Stimuli. Behavioral accuracy for a.) magno-biased clear threat stimuli and b.) parvo-biased ambiguous threat stimuli were predicted by classification accuracy for magno-biased and parvo-biased within the left pars orbitalis.

Figure 11. Regression with Classification Accuracy for Magno-biased/Parvo-biased Stimuli and Behavioral Accuracy for Magno-biased Clear Threat Stimuli. Behavioral accuracy for magno-biased clear threat stimuli was predicted by classification accuracy for magno-biased and parvo-biased within the right amygdala.

Figure 12. Regression with Classification Accuracy for Magno-biased/Parvo-biased Stimuli and Behavioral Accuracy for Magno-biased Threat Stimuli. Behavioral accuracy for a.) magno-biased clear threat stimuli and b.) magno-biased ambiguous threat stimuli were predicted by classification accuracy for magno-biased and parvo-biased within the right hippocampus.

References

Adams, R. B., Gordon, H. L., Baird, A. A., Ambady, N., & Kleck, R. E. (2003). Effects of gaze on amygdala sensitivity to anger and fear faces. *Science*, *300*(5625), 1536-1536.

Adams Jr, R. B., Franklin Jr, R. G., Kveraga, K., Ambady, N., Kleck, R. E., Whalen, P. J., ... & Nelson, A. J. (2011). Amygdala responses to averted vs direct gaze fear vary as a function of presentation speed. *Social Cognitive and Affective Neuroscience*, *7*(5), 568-577.

Adams Jr, R. B., Im, H. I., Cushing, C., Boshyan, J., Ward, N., Albohn, D. N., & Kveraga, K. (2019). *Differential Magnocellular versus Parvocellular Contributions to the Combinatorial Processing of Facial Threat.* In *Progress in brain research* (Vol. 247, pp. 71-87). Elsevier.

Adolphs, R. (2003). Is the human amygdala specialized for processing social information?. *Annals of the New York Academy of Sciences*, *985*(1), 326-340.

Adolphs, R. (2008). Fear, faces, and the human amygdala. *Current opinion in neurobiology*, *18*(2), 166-172.

Adolphs, R., Sears, L., & Piven, J. (2001). Abnormal processing of social information from faces in autism. *Journal of cognitive neuroscience*, *13*(2), 232-240.

Adolphs, R., Tranel, D., Damasio, H., & Damasio, A. R. (1995). Fear and the human amygdala. *Journal of Neuroscience*, *15*(9), 5879-5891.

Ahmadi, K., Pouretemad, H. R., Esfandiari, J., Yoonessi, A., & Yoonessi, A. (2015). Psychophysical evidence for impaired Magno, Parvo, and Konio-cellular pathways in dyslexic children. *Journal of ophthalmic & vision research*, *10*(4), 433.

Ambroggi, F., Ishikawa, A., Fields, H. L., & Nicola, S. M. (2008). Basolateral amygdala neurons facilitate reward-seeking behavior by exciting nucleus accumbens neurons. *Neuron*, *59*(4), 648-661.

Arditi, A. (2005). Improving the design of the letter contrast sensitivity test. *Investigative ophthalmology & visual science*, *46*(6), 2225-2229.

Awasthi, B., Williams, M. A., & Friedman, J. (2016). Examining the role of red background in magnocellular contribution to face perception. *PeerJ*, *4*, e1617.

Bar, M. (2003). A cortical mechanism for triggering top-down facilitation in visual object recognition. *Journal of cognitive neuroscience*, *15*(4), 600-609.

Bar, M., Kassam, K. S., Ghuman, A. S., Boshyan, J., Schmid, A. M., Dale, A. M., ... & Halgren, E. (2006). Top-down facilitation of visual recognition. *Proceedings of the national academy of sciences*, *103*(2), 449-454.

Bar, M., Tootell, R. B., Schacter, D. L., Greve, D. N., Fischl, B., Mendola, J. D., ... & Dale, A. M. (2001). Cortical mechanisms specific to explicit visual object recognition. *Neuron*, *29*(2), 529-535.

Bedwell, J. S., Chan, C. C., Cohen, O., Karbi, Y., Shamir, E., & Rassovsky, Y. (2013). The magnocellular visual pathway and facial emotion misattribution errors in schizophrenia. *Progress in Neuro-Psychopharmacology and Biological Psychiatry*, *44*, 88-93.

Benedek, G., Horváth, G., Kéri, S., Braunitzer, G., & Janáky, M. (2017). The development and aging of the magnocellular and parvocellular visual pathways as indicated by VEP recordings between 5 and 84 years of age. *Vision*, *1*(1), 7.

Bowman, C. R., Chamberlain, J. D., & Dennis, N. A. (2019). Sensory representations supporting memory specificity: Age effects on behavioral and neural discriminability. *Journal of Neuroscience*, *39*(12), 2265-2275.

Boycott, B. B., & Wässle, H. (1991). Morphological classification of bipolar cells of the primate retina. *European Journal of Neuroscience*, *3*(11), 1069-1088.

Brown, A. C., & Crewther, D. P. (2017). Autistic children show a surprising relationship between global visual perception, non-verbal intelligence and visual parvocellular function, not seen in typically developing children. *Frontiers in human neuroscience*, *11*, 239.

Burianová, H., Lee, Y., Grady, C. L., & Moscovitch, M. (2013). Age-related dedifferentiation and compensatory changes in the functional network underlying face processing. *Neurobiology of aging*, *34*(12), 2759-2767.

Bruce, V., & Young, A. (1986). Understanding face recognition. *British journal of psychology*, *77*(3), 305-327.

Burt, A., Hugrass, L., Frith-Belvedere, T., & Crewther, D. (2017). Insensitivity to Fearful Emotion for Early ERP Components in High Autistic Tendency Is Associated with Lower Magnocellular Efficiency. *Frontiers in human neuroscience*, *11*, 495.

Cabeza, R., & Dennis, N. A. (2012). Frontal lobes and aging. *Principles of frontal lobe function. 2d ed. New York: Oxford University Press. p*, 628-652.

Callaway, E. M. (2005). Structure and function of parallel pathways in the primate early visual system. *The Journal of physiology*, *566*(1), 13-19.

Carlezon Jr, W. A., & Thomas, M. J. (2009). Biological substrates of reward and aversion: a nucleus accumbens activity hypothesis. *Neuropharmacology*, *56*, 122-132.

Carp, J., Park, J., Hebrank, A., Park, D. C., & Polk, T. A. (2011a). Age-related neural dedifferentiation in the motor system. *PloS one*, *6*(12).

Carp, J., Park, J., Polk, T. A., & Park, D. C. (2011b). Age differences in neural distinctiveness revealed by multi-voxel pattern analysis. *Neuroimage*, *56*(2), 736-743.

Carretié, L., Hinojosa, J. A., Albert, J., & Mercado, F. (2006). Neural response to sustained affective visual stimulation using an indirect task. *Experimental Brain Research*, *174*(4), 630-637.

Chieffi, S. (2019). Dysfunction of Magnocellular/dorsal Processing Stream in Schizophrenia. *Current Psychiatry Research and Reviews Formerly: Current Psychiatry Reviews*, *15*(1), 26-36.

Chua, E. F., Schacter, D. L., Rand-Giovannetti, E., & Sperling, R. A. (2007). Evidence for a specific role of the anterior hippocampal region in successful associative encoding. *Hippocampus*, *17*(11), 1071-1080.

Collins, A., & Koechlin, E. (2012). Reasoning, learning, and creativity: frontal lobe function and human decision-making. *PLoS Biol*, *10*(3), e1001293.

Cushing, C. A., Im, H. Y., Adams Jr, R. B., Ward, N., & Kveraga, K. (2019). Magnocellular and parvocellular pathway contributions to facial threat cue processing. *Social cognitive and affective neuroscience*, *14*(2), 151-162.

Dale, A. M., Fischl, B., & Sereno, M. I. (1999). Cortical surface-based analysis: I. Segmentation and surface reconstruction. *Neuroimage*, *9*(2), 179-194.

Damasio, A. R., Damasio, H., & Van Hoesen, G. W. (1982). Prosopagnosia: anatomic basis and behavioral mechanisms. *Neurology*, *32*(4), 331-331.

Davis, S. W., Dennis, N. A., Daselaar, S. M., Fleck, M. S., & Cabeza, R. (2007). Que PASA? The posterior–anterior shift in aging. *Cerebral cortex*, *18*(5), 1201-1209.

de Gelder, B., Terburg, D., Morgan, B., Hortensius, R., Stein, D. J., & van Honk, J. (2014). The role of human basolateral amygdala in ambiguous social threat perception. *Cortex*, *52*, 28-34.

De Renzi, E. (1997). Prosopagnosia. In T. Feinberg & M. Farah (Eds.), *Behavioral neurology and neuro-psychology* (pp. 245–255). New York: McGraw-Hill.

Deichmann, R., Gottfried, J. A., Hutton, C., & Turner, R. (2003). Optimized EPI for fMRI studies of the orbitofrontal cortex. *Neuroimage*, *19*(2), 430-441.

Dennis, N. A., & Cabeza, R. (2011). Age-related dedifferentiation of learning systems: an fMRI study of implicit and explicit learning. *Neurobiology of aging*, *32*(12), 2318-e17.

DeMaster, D., Pathman, T., Lee, J. K., & Ghetti, S. (2013). Structural development of the hippocampus and episodic memory: developmental differences along the anterior/posterior axis. *Cerebral cortex*, *24*(11), 3036-3045.

Desikan, R. S., Ségonne, F., Fischl, B., Quinn, B. T., Dickerson, B. C., Blacker, D., ... & Albert, M. S. (2006). An automated labeling system for subdividing the human cerebral cortex on MRI scans into gyral based regions of interest. *Neuroimage*, *31*(3), 968-980.

Denison, R. N., Vu, A. T., Yacoub, E., Feinberg, D. A., & Silver, M. A. (2014). Functional mapping of the magnocellular and parvocellular subdivisions of human LGN. *Neuroimage*, *102*, 358-369.

Duchaine, B., & Yovel, G. (2015). A revised neural framework for face processing. *Annual Review of Vision Science*, *1*, 393-416.

Ebner, N. C., Riediger, M., & Lindenberger, U. (2010). FACES—A database of facial expressions in young, middle-aged, and older women and men: Development and validation. *Behavior research methods*, *42*(1), 351-362.

Ekman, P., & Freisen, W. V. (1975) Pictures of facial affect. *Consulting Psychologists Press.*

Elbich, D. B., & Scherf, S. (2017). Beyond the FFA: brain-behavior correspondences in face recognition abilities. *Neuroimage*, *147*, 409-422.

Elbich, D. B., Molenaar, P. C., & Scherf, K. S. (2019). Evaluating the organizational structure and specificity of network topology within the face processing system. *Human brain mapping*, *40*(9), 2581-2595.

Felleman, D. J., & Van, D. E. (1991). Distributed hierarchical processing in the primate cerebral cortex. *Cerebral cortex (New York, NY: 1991)*, *1*(1), 1-47.

Fellows, L. K. (2006). Deciding how to decide: ventromedial frontal lobe damage affects information acquisition in multi-attribute decision making. *Brain*, *129*(4), 944-952.

Fellows, L. K., & Farah, M. J. (2005). Different underlying impairments in decision-making following ventromedial and dorsolateral frontal lobe damage in humans. *Cerebral cortex*, *15*(1), 58-63.

Fischl, B., & Dale, A. M. (2000). Measuring the thickness of the human cerebral cortex from magnetic resonance images. *Proceedings of the National Academy of Sciences*, *97*(20), 11050-11055.

Fischl, B., Rajendran, N., Busa, E., Augustinack, J., Hinds, O., Yeo, B. T., ... & Zilles, K. (2008). Cortical folding patterns and predicting cytoarchitecture. *Cerebral cortex*, *18*(8), 1973-1980.

Fischl, B., Salat, D. H., Busa, E., Albert, M., Dieterich, M., Haselgrove, C., ... & Montillo, A. (2002). Whole brain segmentation: automated labeling of neuroanatomical structures in the human brain. *Neuron*, *33*(3), 341-355.

Fischl, B., Sereno, M. I., Tootell, R. B., & Dale, A. M. (1999). High-resolution intersubject averaging and a coordinate system for the cortical surface. *Human brain mapping*, *8*(4), 272-284.

Fischl, B. (2012). FreeSurfer. *Neuroimage*, *62*(2), 774-781.

Ganel, T., Valyear, K. F., Goshen-Gottstein, Y., & Goodale, M. A. (2005). The involvement of the "fusiform face area" in processing facial expression. *Neuropsychologia*, *43*(11), 1645-1654.

Gauthier, I., & Nelson, C. A. (2001). The development of face expertise. *Current opinion in neurobiology*, *11*(2), 219-224.

Gori, S., Seitz, A. R., Ronconi, L., Franceschini, S., & Facoetti, A. (2016). Multiple causal links between magnocellular–dorsal pathway deficit and developmental dyslexia. *Cerebral Cortex*, *26*(11), 4356-4369.

Harry, B. B., Williams, M., Davis, C., & Kim, J. (2013). Emotional expressions evoke a differential response in the fusiform face area. *Frontiers in human neuroscience*, *7*, 692.

Lehmann, M., Douiri, A., Kim, L. G., Modat, M., Chan, D., Ourselin, S., ... & Fox, N. C. (2010). Atrophy patterns in Alzheimer's disease and semantic dementia: a comparison of FreeSurfer and manual volumetric measurements. *Neuroimage*, *49*(3), 2264-2274.

Hebb, D. O. (1949). *The organization of behavior: A neuropsychological approach*. John Wiley & Sons.

Friston, K. J., Harrison, L., & Penny, W. (2003). Dynamic causal modelling. *Neuroimage*, *19*(4), 1273-1302.

Furl, N., Garrido, L., Dolan, R. J., Driver, J., & Duchaine, B. (2011). Fusiform gyrus face selectivity relates to individual differences in facial recognition ability. *Journal of Cognitive Neuroscience*, *23*(7), 1723-1740.

Gilmore, G. C., Wenk, H. E., Naylor, L. A., & Koss, E. (1994). Motion perception and Alzheimer's disease. *Journal of Gerontology*, *49*(2), P52-P57.

Gobbini, M. I., & Haxby, J. V. (2007). Neural systems for recognition of familiar faces. *Neuropsychologia*, *45*(1), 32-41.

Goodale, M. A., & Milner, A. D. (1992). Separate visual pathways for perception and action.

Grill-Spector, K., Kourtzi, Z., & Kanwisher, N. (2001). The lateral occipital complex and its role in object recognition. *Vision research*, *41*(10-11), 1409-1422.

Gur, R. C., Schroeder, L., Turner, T., McGrath, C., Chan, R. M., Turetsky, B. I., ... & Gur, R. E. (2002). Brain activation during facial emotion processing. *Neuroimage*, *16*(3), 651-662.

Habel, U., Windischberger, C., Derntl, B., Robinson, S., Kryspin-Exner, I., Gur, R. C., & Moser, E. (2007). Amygdala activation and facial expressions: explicit emotion discrimination versus implicit emotion processing. *Neuropsychologia*, *45*(10), 2369-2377.

Haxby, J. V., Gobbini, M. I., Furey, M. L., Ishai, A., Schouten, J. L., & Pietrini, P. (2001). Distributed and overlapping representations of faces and objects in ventral temporal cortex. *Science*, *293*(5539), 2425-2430.

Haxby, J. V., Hoffman, E. A., & Gobbini, M. I. (2000). The distributed human neural system for face perception. *Trends in cognitive sciences*, *4*(6), 223-233.

Huang, L., Song, Y., Li, J., Zhen, Z., Yang, Z., & Liu, J. (2014). Individual differences in cortical face selectivity predict behavioral performance in face recognition. *Frontiers in human neuroscience*, *8*, 483.

Hooker, C., & Park, S. (2002). Emotion processing and its relationship to social functioning in schizophrenia patients. *Psychiatry research*, *112*(1), 41-50.

Im, H. Y., Adams, R. B., Boshyan, J., Ward, N., Cushing, C. A., & Kveraga, K. (2017). Observer's anxiety facilitates magnocellular processing of clear facial threat cues, but impairs parvocellular processing of ambiguous facial threat cues. *Scientific reports*, *7*(1), 15151.

Im, H. Y., Adams Jr, R. B., Cushing, C. A., Boshyan, J., Ward, N., & Kveraga, K. (2018). Sex-related differences in behavioral and amygdalar responses to compound facial threat cues. *Human brain mapping*, *39*(7), 2725-2741.

Ishai, A., Ungerleider, L. G., & Haxby, J. V. (2000). Distributed neural systems for the generation of visual images. *Neuron*, *28*(3), 979-990.

Ishihara, S. (1917). *Tests for Color blindness*.

Kadosh, K. C., & Johnson, M. H. (2007). Developing a cortex specialized for face perception. *Trends in Cognitive Sciences*, *11*(9), 367-369.

Kanwisher, N., McDermott, J., & Chun, M. M. (1997). The fusiform face area: a module in human extrastriate cortex specialized for face perception. *Journal of neuroscience*, *17*(11), 4302-4311.

Kaplan, E. (2004). The M, P, and K pathways of the primate visual system. In L. M. Chalupa & J. S. Werner (Eds.), *The visual neurosciences* (pp. 481-494). Cambridge, MA: The MIT Press.

Kaplan, E., & Shapley, R. M. (1986). The primate retina contains two types of ganglion cells, with high and low contrast sensitivity. *Proceedings of the National Academy of Sciences*, *83*(8), 2755-2757.

Kim, D., Wylie, G., Pasternak, R., Butler, P. D., & Javitt, D. C. (2006). Magnocellular contributions to impaired motion processing in schizophrenia. *Schizophrenia research*, *82*(1), 1-8.

Kosaka, H., Omori, M., Murata, T., Iidaka, T., Yamada, H., Okada, T., ... & Wada, Y. (2002). Differential amygdala response during facial recognition in patients with schizophrenia: an fMRI study. *Schizophrenia research*, *57*(1), 87-95.

Kriegeskorte, N., Formisano, E., Sorger, B., & Goebel, R. (2007). Individual faces elicit distinct response patterns in human anterior temporal cortex. *Proceedings of the National Academy of Sciences*, *104*(51), 20600-20605.

Kveraga, K., Ghuman, A. S., & Bar, M. (2007a). Top-down predictions in the cognitive brain. *Brain and cognition*, *65*(2), 145-168.

Kveraga, K., Boshyan, J., & Bar, M. (2007b). Magnocellular projections as the trigger of top-down facilitation in recognition. *Journal of Neuroscience*, *27*(48), 13232-13240.

Kveraga, K. (2014). Threat perception in visual scenes: Dimensions, action and neural dynamics. *Scene Vision: making sense of what we see*, 291-307.

Kveraga, K. et al. Visual pathway contributions to affective scene perception. Organization for Human Brain Mapping (2015).

Lawton, T. (2016). Improving dorsal stream function in dyslexics by training figure/ground motion discrimination improves attention, reading fluency, and working memory. *Frontiers in human neuroscience*, *10*, 397.

Lhermitte, F., Chain, F., Escourolle, R., Ducarne, B., & Pillon, B. (1972). Anatomoclinical study of a case of prosopagnosia. *Revue neurologique*, *126*(5), 329.

Mahmoudi, A., Takerkart, S., Regragui, F., Boussaoud, D., & Brovelli, A. (2012). Multivoxel pattern analysis for FMRI data: a review. *Computational and mathematical methods in medicine*, *2012*.

Martínez, A., Hillyard, S. A., Dias, E. C., Hagler, D. J., Butler, P. D., Guilfoyle, D. N., ... & Javitt, D. C. (2008). Magnocellular pathway impairment in schizophrenia: evidence from functional magnetic resonance imaging. *Journal of Neuroscience*, *28*(30), 7492-7500.

Martins, B., Ponzio, A., Velasco, R., Kaplan, J., & Mather, M. (2014). Dedifferentiation of emotion regulation strategies in the aging brain. *Social cognitive and affective neuroscience*, *10*(6), 840-847.

Mazaika, P., Hoeft, F., Glover, G., H., & Reiss, A. L. (2009). *Methods and Software for fMRI Analysis for Clinical Subjects*. [Conference Presentation] Human Brain Mapping 2009 Convention.

McCleery, J. P., Allman, E., Carver, L. J., & Dobkins, K. R. (2007). Abnormal magnocellular pathway visual processing in infants at risk for autism. *Biological psychiatry*, *62*(9), 1007-1014.

McFayden, T. C., Albright, J., Muskett, A. E., & Scarpa, A. (2019). Brief Report: Sex Differences in ASD Diagnosis—A Brief Report on Restricted Interests and Repetitive Behaviors. *Journal of autism and developmental disorders*, *49*(4), 1693-1699.

Meadows, J. C. (1974). The anatomical basis of prosopagnosia. *Journal of Neurology, Neurosurgery & Psychiatry*, *37*(5), 489-501.

Merigan, W. H., & Maunsell, J. H. (1993). How parallel are the primate visual pathways?. *Annual review of neuroscience*, *16*(1), 369-402.

Milders, M., Hietanen, J. K., Leppänen, J. M., & Braun, M. (2011). Detection of emotional faces is modulated by the direction of eye gaze. *Emotion*, *11*(6), 1456.

Mishkin, M., Ungerleider, L. G., & Macko, K. A. (1983). Object vision and spatial vision: two cortical pathways. *Trends in neurosciences*, *6*, 414-417.

Mueller, S. G., Chao, L. L., Berman, B., & Weiner, M. W. (2011). Evidence for functional specialization of hippocampal subfields detected by MR subfield volumetry on high resolution images at 4 T. *Neuroimage*, *56*(3), 851-857.

Mundel, T., Milton, J. G., Dimitrov, A., Wilson, H. W., Pelizzari, C., Uftring, S., ... & Towle, V. L. (2003). Transient inability to distinguish between faces: electrophysiologic studies. *Journal of clinical neurophysiology*, *20*(2), 102-110.

Murav'eva, S. V., Deshkovich, A. A., & Shelepin, Y. E. (2009). The human magno and parvo systems and selective impairments of their functions. *Neuroscience and behavioral physiology*, *39*(6), 535-543.

Norman, K. A., Polyn, S. M., Detre, G. J., & Haxby, J. V. (2006). Beyond mind-reading: multi-voxel pattern analysis of fMRI data. *Trends in cognitive sciences*, *10*(9), 424-430.

Norton, D., McBain, R., Holt, D. J., Ongur, D., & Chen, Y. (2009). Association of impaired facial affect recognition with basic facial and visual processing deficits in schizophrenia. *Biological Psychiatry*, *65*(12), 1094-1098.

Ofen, N., Kao, Y. C., Sokol-Hessner, P., Kim, H., Whitfield-Gabrieli, S., & Gabrieli, J. D. (2007). Development of the declarative memory system in the human brain. *Nature neuroscience*, *10*(9), 1198.

Ojemann, J. G., Akbudak, E., Snyder, A. Z., McKinstry, R. C., Raichle, M. E., & Conturo, T. E. (1997). Anatomic localization and quantitative analysis of gradient refocused echo-planar fMRI susceptibility artifacts. *Neuroimage*, *6*(3), 156-167.

Olton, D. S., & Paras, B. C. (1979). Spatial memory and hippocampal function. *Neuropsychologia*, *17*(6), 669-682.

O'Toole, A. J., Jiang, F., Abdi, H., & Haxby, J. V. (2005). Partially distributed representations of objects and faces in ventral temporal cortex. *Journal of cognitive neuroscience*, *17*(4), 580-590.

Orban, G. A., Van Essen, D., & Vanduffel, W. (2004). Comparative mapping of higher visual areas in monkeys and humans. *Trends in cognitive sciences*, *8*(7), 315-324.

Papenberg, G., Bäckman, L., Chicherio, C., Nagel, I. E., Heekeren, H. R., Lindenberger, U., & Li, S. C. (2011). Higher intraindividual variability is associated with more forgetting and dedifferentiated memory functions in old age. *Neuropsychologia*, *49*(7), 1879-1888.

Park, D. C., & Reuter-Lorenz, P. (2009). The adaptive brain: aging and neurocognitive scaffolding. *Annual review of psychology*, *60*, 173-196.

Park, D. C., Polk, T. A., Park, R., Minear, M., Savage, A., & Smith, M. R. (2004). Aging reduces neural specialization in ventral visual cortex. *Proceedings of the National Academy of Sciences*, *101*(35), 13091-13095.

Park, J., Carp, J., Kennedy, K. M., Rodrigue, K. M., Bischof, G. N., Huang, C. M., ... & Park, D. C. (2012). Neural broadening or neural attenuation? Investigating age-related dedifferentiation in the face network in a large lifespan sample. *Journal of Neuroscience*, *32*(6), 2154-2158.

Peelen, M. V., Glaser, B., Vuilleumier, P., & Eliez, S. (2009). Differential development of selectivity for faces and bodies in the fusiform gyrus. *Developmental science*, *12*(6), F16-F25.

Perry, V. H., Oehler, R., & Cowey, A. (1984). Retinal ganglion cells that project to the dorsal lateral geniculate nucleus in the macaque monkey. *Neuroscience*, *12*(4), 1101-1123.

Pillay, S. S., Gruber, S. A., Rogowska, J., Simpson, N., & Yurgelun-Todd, D. A. (2006). fMRI of fearful facial affect recognition in panic disorder: the cingulate gyrus–amygdala connection. *Journal of affective disorders*, *94*(1-3), 173-181.

Poldrack, R. A., Clark, J., Pare-Blagoev, E. J., Shohamy, D., Moyano, J. C., Myers, C., & Gluck, M. A. (2001). Interactive memory systems in the human brain. *Nature*, *414*(6863), 546.

Puce, A., Allison, T., Gore, J. C., & McCarthy, G. (1995). Face-sensitive regions in human extrastriate cortex studied by functional MRI. *Journal of neurophysiology*, *74*(3), 1192-1199.

Salimpoor, V. N., van den Bosch, I., Kovacevic, N., McIntosh, A. R., Dagher, A., & Zatorre, R. J. (2013). Interactions between the nucleus accumbens and auditory cortices predict music reward value. *Science*, *340*(6129), 216-219.

Sato, W., Yoshikawa, S., Kochiyama, T., & Matsumura, M. (2004). The amygdala processes the emotional significance of facial expressions: an fMRI investigation using the interaction between expression and face direction. *Neuroimage*, *22*(2), 1006-1013.

Schacter, D. L., & Wagner, A. D. (1999). Medial temporal lobe activations in fMRI and PET studies of episodic encoding and retrieval. *Hippocampus*, *9*(1), 7-24.

Scoville, W. B., & Milner, B. (1957). Loss of recent memory after bilateral hippocampal lesions. *Journal of neurology, neurosurgery, and psychiatry*, *20*(1), 11.

Senior, C., Ward, J., & David, A. S. (2002). Representational momentum and the brain: An investigation into the functional necessity of V5/MT. *Visual Cognition*, *9*(1-2), 81-92.

Squire, L. R., & Wixted, J. T. (2011). The cognitive neuroscience of human memory since HM. *Annual review of neuroscience*, *34*, 259-288.

Sutherland, A., & Crewther, D. P. (2010). Magnocellular visual evoked potential delay with high autism spectrum quotient yields a neural mechanism for altered perception. *Brain*, *133*(7), 2089-2097.

Thomas, C., Kveraga, K., Huberle, E., Karnath, H. O., & Bar, M. (2012). Enabling global processing in simultanagnosia by psychophysical biasing of visual pathways. *Brain*, *135*(5), 1578-1585.

Tobimatsu, S., Tomoda, H., & Kato, M. (1996). Human VEPs to isoluminant chromatic and achromatic sinusoidal gratings: separation of parvocellular components. *Brain topography*, *8*(3), 241-243.

Tottenham, N., Tanaka, J. W., Leon, A. C., McCarry, T., Nurse, M., Hare, T. A., ... & Nelson, C. (2009). The NimStim set of facial expressions: judgments from untrained research participants. *Psychiatry research*, *168*(3), 242-249.

Tootell, R. B., Hadjikhani, N. K., Vanduffel, W., Liu, A. K., Mendola, J. D., Sereno, M. I., & Dale, A. M. (1998). Functional analysis of primary visual cortex (V1) in humans. *Proceedings of the National Academy of Sciences*, *95*(3), 811-817.

Tustison, N. J., Cook, P. A., Klein, A., Song, G., Das, S. R., Duda, J. T., ... & Avants, B. B. (2014). Large-scale evaluation of ANTs and FreeSurfer cortical thickness measurements. *Neuroimage*, *99*, 166-179.

Qiu, F. T., & Von Der Heydt, R. (2005). Figure and ground in the visual cortex: V2 combines stereoscopic cues with Gestalt rules. *Neuron*, *47*(1), 155-166.

Snellen, H. (1862). *Probebuchstaben zur Bestimmung der Sehschärfe*.

Ungerleider, L. G., & Haxby, J. V. (1994). 'What' and 'where' in the human brain. *Current opinion in neurobiology*, *4*(2), 157-165.

Vidyasagar, T. R., & Pammer, K. (1999). Impaired visual search in dyslexia relates to the role of the magnocellular pathway in attention. *Neuroreport*, *10*(6), 1283-1287.

Vidyasagar, T. R., & Pammer, K. (2010). Dyslexia: a deficit in visuo-spatial attention, not in phonological processing. *Trends in cognitive sciences*, *14*(2), 57-63.

Vogels, R., Biederman, I., Bar, M., & Lorincz, A. (2001). Inferior temporal neurons show greater sensitivity to nonaccidental than to metric shape differences. *Journal of Cognitive Neuroscience*, *13*(4), 444-453.

Voss, M. W., Erickson, K. I., Chaddock, L., Prakash, R. S., Colcombe, S. J., Morris, K. S., ... & Kramer, A. F. (2008). Dedifferentiation in the visual cortex: an fMRI investigation of individual differences in older adults. *Brain research*, *1244*, 121-131.

Vuilleumier, P., Armony, J. L., Driver, J., & Dolan, R. J. (2003). Distinct spatial frequency sensitivities for processing faces and emotional expressions. *Nature neuroscience*, *6*(6), 624-631.

Vuilleumier, P., & Pourtois, G. (2007). Distributed and interactive brain mechanisms during emotion face perception: evidence from functional neuroimaging. *Neuropsychologia*, *45*(1), 174-194.

Wada, Y., & Yamamoto, T. (2001). Selective impairment of facial recognition due to a haematoma restricted to the right fusiform and lateral occipital region. *Journal of Neurology, Neurosurgery & Psychiatry*, *71*(2), 254-257.

Wang, B. (2013). Facial expression influences recognition memory for faces: Robust enhancement effect of fearful expression. *Memory*, *21*(3), 301-314.

Yang, J., Xu, X., Du, X., Shi, C., & Fang, F. (2011). Effects of unconscious processing on implicit memory for fearful faces. *PloS one*, *6*(2).

Yoonessi, A., & Yoonessi, A. (2011). Functional assessment of magno, parvo and konio-cellular pathways; current state and future clinical applications. *Journal of ophthalmic & vision research*, *6*(2), 119.

Zeki, S. M. (1978). Uniformity and diversity of structure and function in rhesus monkey prestriate visual cortex. *The Journal of Physiology*, *277*(1), 273-290.

Daniel B. Elbich
Curriculum Vitae
dbe5007@psu.edu

Education

2020	**Ph D (Psychology)** The Pennsylvania State University
2016	**M.S. (Psychology)** The Pennsylvania State University
2011	**B.S. (Psychology)** The Pennsylvania State University

Published Manuscripts

Frith, E., **Elbich, D.B.**, Christensen, A.P., Rosenberg, M.D., Chen, Q., Silvia, P.J., Seli, P, & Beaty, R.E. (accepted). *Intelligence and Creativity Share a Common Cognitive and Neural Basis.*

Elbich, D.B., Molenaar, P.C., & Scherf, K.S. (2019). *Evaluating the Organizational Structure and Specificity of Network Topology within the Face Processing System.* Human Brain Mapping, 1-15. https://doi.org/10.1002/hbm.24546

Scherf, K.S., Griffin, J, Judy, B., Whyte, E., Geier, C., **Elbich, D.**, Smyth, J. (2018) *Improving Sensitivity to Eye Gaze Cues in Autism Using Serious Game Technology: Study Protocol for a Phase I Randomized Controlled Trial*. BMJ Open, 8, e023682. http://dx.doi.org/10.1136/bmjopen-2018-023682

Scherf, K.S., **Elbich, D.B.,** & Motta-Mena, N.V. (2017). *Investigating the Influence of Biological Sex on the Behavioral and Neural Basis of Face Recognition.* eNeuro, 4, 1-18. https://dx.doi.org/10.1523%2FENEURO.0104-17.2017

Elbich, D.B. & Scherf, K.S. (2017). *Beyond the FFA: Brain-Behavior Correspondences in Face Recognition Abilities.* NeuroImage, 147, 409-422. https://doi.org/10.1016/j.neuroimage.2016.12.042

Scherf, K.S., **Elbich, D.,** Minshew, N., & Behrmann, M. (2015). *Individual Differences in Symptom Severity and Behavior Predict Neural Activation During Face Processing in Adolescents with Autism.* NeuroImage: Clinical, 7, 53-67. https://doi.org/10.1016/j.nicl.2014.11.003

Research Experience

Part-Time Project Support, Cognitive and Mobile Phenotyping Neurolaboratory, Dr. Jonathan Hakun, 02/2020-06/2020

Graduate Research Assistant, Cognitive, Aging, and Neuroscience Lab, Dr. Nancy Dennis, 08/2018-06/2020

Graduate Research Assistant, Laboratory of Developmental Neuroscience, Dr. Suzy Scherf, 08/2013-8/2018

Research Coordinator, Laboratory of Developmental Neuroscience, Dr. Suzy Scherf, 08/2011-07/2013

Select Honors & Awards

College of Liberal Arts Superior Teaching and Research (STAR) Award, 2016

Dept. of Psychology Graduate Travel Award, 2013-2018